Seasonal variations and controlling factors of nitrogen fluxes at the sediment-water interface in a semi-enclosed inland sea

Zhaosen Wu[1, 2], Xinyu Guo[2, *], Jie Shi[1, 3], Xiaokun Ding[4], Masatoshi Nakakuni[5, 6], Kuninao Tada[5, 6]

[1]Key Laboratory of Marine Environment and Ecology, Ministry of Education of China, Ocean University of China, 238 Songling Road, Qingdao 266100, China

[2]Center for Marine Environmental Studies, Ehime University, 2-5 Bunkyo-Cho, Matsuyama 790-8577, Japan

[3]Laboratory for Marine Ecology and Environmental Sciences, Qingdao National Laboratory for Marine Science and Technology, Qingdao, 266071, China

[4]School of Ocean, Yantai University, Yantai, 264005, China

[5]Faculty of Agriculture, Kagawa University, Ikenobe, Kita, Miki, Kagawa 761-0701, Japan

[6]Seto Inland Sea Regional Research Center, Kagawa University, Saiwai, Takamatsu, Kagawa 761-0016, Japan

Corresponding to: Xinyu Guo (guo.xinyu.mz@ehime-u.ac.jp) ORCID: 0000-0002-4832-8625

Abstract. Nitrogen fluxes across the sediment-water interface and nitrogen removal from sediments are essential components of the nitrogen cycle and ecosystem in semi-enclosed inland seas. However, the difficulty in observational sampling hinders the acquisition of continuous data necessary to understand their seasonal variations and underlying mechanisms. In response to this issue, we have developed a one-dimensional vertical model of the nitrogen cycle within sediments and used it to reproduce the seasonal changes of observed nitrogen fluxes in a typical semi-enclosed inland sea and investigate their controlling factors through sensitivity experiments. Model results indicate that ~~40~~48% of particulate organic nitrogen (PON) settling into sediments is returned to the bottom water as dissolved inorganic nitrogen (DIN), while ~~30~~6% is removed via N-loss flux (dinitrogen gas and nitrous oxide). ~~Although~~ The seasonal variations of PON ~~flux is controlled~~and DIN fluxes are governed by ~~PON concentration in~~ fundamentally different environmental factors, highlighting the necessity of accounting for seasonal changes in bottom ~~-~~water~~, DIN and N-loss fluxes show~~ temperature ~~driven seasonal variations, suggesting a decoupling between~~ and nitrogen ~~return and PON input. Additionally, seasonal variations~~ concentrations when estimating DIN flux in ~~oxygen penetration depth (OPD), ranging from 1 to 3 mm, also affect nitrogen fluxes. In nitrate depleted sediments of semi enclosed seas,~~ the sediment–water interface. Nitrogen

removal is dominated by denitrification~~ rate is no longer significantly higher than~~. However, its overall magnitude remains relatively low, constrained by the ~~anammox rate~~oligotrophic conditions in ~~the nitrogen removal.~~our study site.

Keywords: sediment-water interface, semi-enclosed inland sea, nitrogen fluxes, sediment model, nitrogen removal

1 Introduction

Sediments play a crucial role in regulating the storage and removal of nitrogen within semi-enclosed inland seas, which significantly influences the balance and stability of the ecosystem (Huettel et al., 2014; Zhang et al., 2020; Kalvelage et al., 2013; Thamdrup, 2012). On one hand, the sediment can bury substantial amounts of nitrogen, potentially on par with river inputs (Liu et al., 2021; Han et al., 2021; Lønborg and Markager, 2021). On the other hand, because of remineralization, the sediment continuously releases dissolved inorganic nitrogen (DIN) into the overlying water (Devol, 2015; Boynton et al., 2017; Liu et al., 2012). In the semi-enclosed inland sea, vertical mixing facilitates the contribution of DIN from sediments as a vital nutrient source for primary production because of shallow water depth (Huettel et al., 2014; Yi et al., 2023; Leng et al., 2023; Liu and Yin, 2007; Berelson et al., 2013; Leynaert et al., 2011; Mei Liu et al., 2011). Notably, the sediment serves as the primary anoxic environment in these regions, where key nitrogen removal processes, such as denitrification and anammox, occur. These processes are essential for regulating nitrogen inventories and influencing nutrient structure in these areas. Researches indicate that continental shelves, which constitute merely 7.5% of the global seafloor, are responsible for 44% of fixed nitrogen losses (Devol, 2015; Mctigue et al., 2016; Huang et al., 2021; Jäntti and Hietanen, 2012; Khalil and Rasmussen, 2012). Furthermore, nitrous oxide, a byproduct of denitrification, is a significant greenhouse gas that contributes to global warming (Wilson et al., 2020; Yang et al., 2022).

To clarify the function of the sediment in ecological and environmental changes, it is necessary to conduct a quantitative analysis of nitrogen fluxes at the sediment-water interface in semi-enclosed inland seas, along with their seasonal variations. Direct observation of particulate organic nitrogen (PON) flux at this interface poses challenges due to the influence of resuspension processes. Consequently, numerous studies focused on DIN flux and its seasonal variations primarily through in situ observations, incubation experiments, or estimations based on Fick's law (De Vittor et al., 2012; Mu et al., 2017; Chen et al., 2023). For example, studies in the northern Adriatic Sea and the Baltic Sea have demonstrated the same conclusion that DIN flux exhibits seasonal variations, with higher levels in summer and lower levels in winter, likely influenced by water temperature (De Vittor et al., 2012; Niemistö et al., 2018). The fluxes of dinitrogen gas and nitrous oxide are mainly accessed through the measurement of denitrification and anammox rates within sediments (Zhang et al., 2018; Rich et al., 2020). A study conducted in the Pearl

River Estuary reported that the denitrification rate in sediments also displayed seasonal variability, with peak values observed in summer and reduced values in winter (Teng and Lin, 2024). However, the challenges and cost associated with field sampling limit the feasibility of continuous monitoring of these fluxes. Moreover, the direction of DIN flux varies across different regions, with the underlying mechanisms remaining unclear (Mu et al., 2017; De Vittor et al., 2015; Dale et al., 2022; Bohlen et al., 2011; Ratmaya et al., 2022; Zhou et al., 2022). Therefore, identifying the magnitude and direction of nitrogen fluxes at the sediment-water interface in semi-enclosed inland seas, along with their seasonal patterns and underlying controlling mechanisms, is crucial for understanding the contribution of sediments to the aquatic ecosystem in ~~this region~~these regions.

Numerical modelling is a valuable tool for understanding the factors that govern nitrogen fluxes at the sediment-water interface. Typically, nitrogen fluxes at this interface derived from empirical formulas serve as essential boundary conditions for modelling the aquatic nitrogen cycle in semi-enclosed inland seas (Lønborg and Markager, 2021). However, this approach largely overlooks the changes occurring within the sediment and the corresponding flux responses to these alterations. An alternative approach is the implementation of a box model, which investigates nitrogen processes within the sediment. Nonetheless, the box model's treatment of all sediment as a single domain, coupled with its failure to account for the vertical distribution of chemical substances—particularly oxidants such as dissolved oxygen (DO)—limits its capacity to provide a comprehensive understanding of the nitrogen cycling processes within the sediment (Yang et al., 2022). A one-dimensional vertical sediment model addresses this limitation, albeit at the cost of increased complexity and computational demands. This model has demonstrated efficacy in accurately reproducing seasonal variations in nitrogen fluxes at the sediment-water interface (Radtke et al., 2019; Umlauf et al., 2023). Despite the clear advantages of this modelling approach over empirical formulas and box models, well-validated applications remain relatively scarce.

This study focuses on the unclear seasonal variations in the magnitude and direction of nitrogen fluxes at the sediment–water interface in semi-enclosed inland seas, alongside the insufficiently understood underlying mechanisms with controlling factors driving these changes. We developed a one-dimensional vertical sediment model to simulate nitrogen cycling and accurately quantify nitrogen fluxes at the interface. Supported by monthly continuous observations conducted in the bottom water and sediment of Harima Nada in Japan, a typical semi-enclosed inland sea, we obtained a robust dataset for model

validation. The model successfully reproduced the seasonal variations in the concentrations of three nitrogen species within the sediment and nitrogen fluxes at the sediment-water interface. Additionally, numerical experiments further elucidated the influence of key environmental factors on these seasonal variations. This study aspires to establish a scientific foundation for comprehending the role of sediment nitrogen cycling in influencing the ecological environment of semi-enclosed marine systems. The findings can provide crucial support for offshore environmental remediation and the development of management policies.

2 Materials and Methods

2.1 Study area

Harima Nada is situated within Seto Inland Sea, the largest semi-enclosed sea in Japan (Figure 1). It has an average water depth of 26 meters and is connected to Osaka Bay and Hiuchi Nada on the eastern and western sides, respectively. To the south, it connects to the Pacific Ocean through the Naruto Strait and Kii Channel (Zhu et al., 2019; Chang et al., 2009). Harima Nada is strongly controlled by seasonal variations in wind forcing and density structure (Tong-u-dom et al., 2023). Its hydrographic circulation exhibits clear seasonal patterns: in winter, a wind-driven downwind circulation dominates under the prevailing north-westerly winds, whereas in summer, a density-driven cyclonic circulation develops due to the horizontal change in stratification. The water column structure also shows pronounced seasonality. Stratification intensifies in summer, promoting the formation of bottom cold water, while in winter, the water column becomes vertically well mixed. These seasonal changes in circulation and stratification jointly regulate the spatial distribution of temperature, salinity, and currents within the basin.

Based on the dataset from the Japanese Ministry of the Environment (https://water-pub.env.go.jp/water-pub/mizu-site/mizu/kouiki/dataMap.asp), DO concentrations in Harima Nada range from 6 to 10 mg L^{-1} (Figure S1). Surface DO exhibits clear seasonal variability, with the lowest values observed in autumn and the highest in winter. Controlled by hydrodynamic conditions, bottom DO reach its minimum in summer due to the intensification of stratification, while vertical mixing in winter leads to the highest bottom DO concentrations.

Chlorophyll concentrations and primary production in the water column are primarily regulated by nutrient availability (Leng et al., 2023; Tong-u-dom et al., 2025). During summer, elevated chlorophyll levels are observed in the estuarine region due to increased riverine nutrient input (Figure S2). In autumn and winter, enhanced vertical mixing redistributes DO, promoting higher chlorophyll concentrations in bottom waters. Previous study has estimated the annual primary production in Harima Nada to be approximately 41 g N m^{-2} yr^{-1} (Tada, 2021). As moving to the sea bottom, most of the sediments in the Harima Nada are muddy, with a mud content exceeding 70%.

Over the past several decades, the environment of the Seto Inland Sea has undergone significant changes (Ishii et al., 2014; Yamamoto et al., 2021). With the continuous observations of sediments in Harima Nada by our collaborators, we have realized that the DIN input from sediments in this area is comparable to that from rivers, exhibiting notable seasonal variations (Leng et al., 2023; Nakakuni et al., 2024). However, the driving factors and mechanisms behind these seasonal changes remain unclear. Therefore, Harima Nada serves as an excellent study area, and these observational data can provide a sufficient validation to ensure the reliability of model results (Nakakuni et al., 2024). This allows us to examine the seasonal variations in sediment nitrogen cycling and interfacial nitrogen fluxes, as well as their controlling mechanisms. Additionally, this study lays the groundwork for future exploration of how sediment nitrogen cycling responds to long-term changes in the aquatic environment.

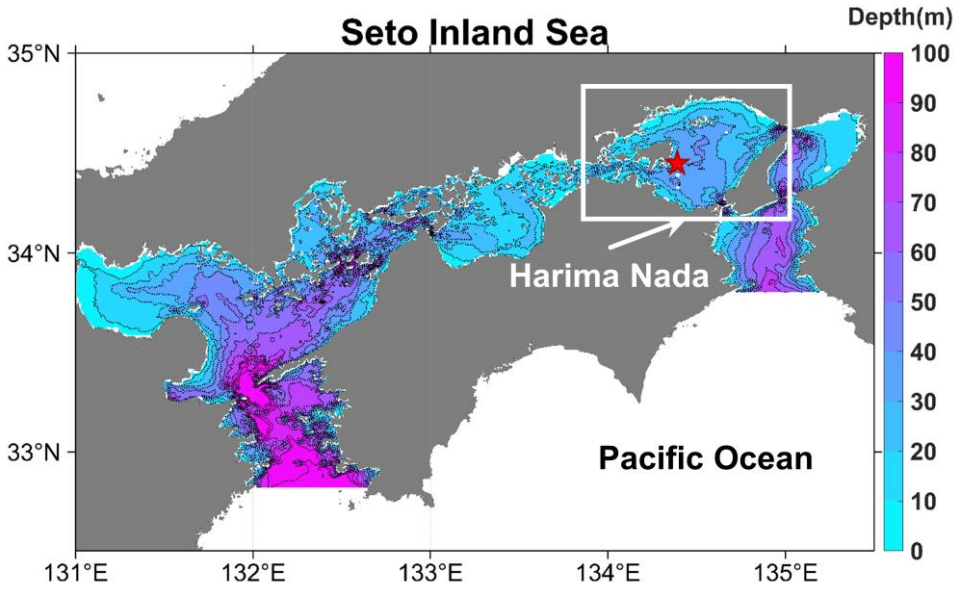

Figure 1. Study area of the Harima Nada, Japan. The red star represents the site where the observational data used in this study were collected.

2.2 Model descriptions

Based on the theory of early diagenesis (Berner, 1980), we have developed a biogeochemical model for sediment (Figure ~~1~~2). This model encompasses two components: solid matter and pore water. The state variables consist of the concentrations of two types of PON (fast-decayed and slow-decayed ones) for the solid matter and the concentrations of NH_4^+ ~~and~~, NO_2^-, NO_3^-, DO and ODU (the oxygen demand units) in the pore water. Additionally, we set a fluff layer at the top of sediment, where the active benthos and material exchange processes with the above water column occur (Lee et al., 2002; Kuhrts et al., 2006; Laima et al., 2002).

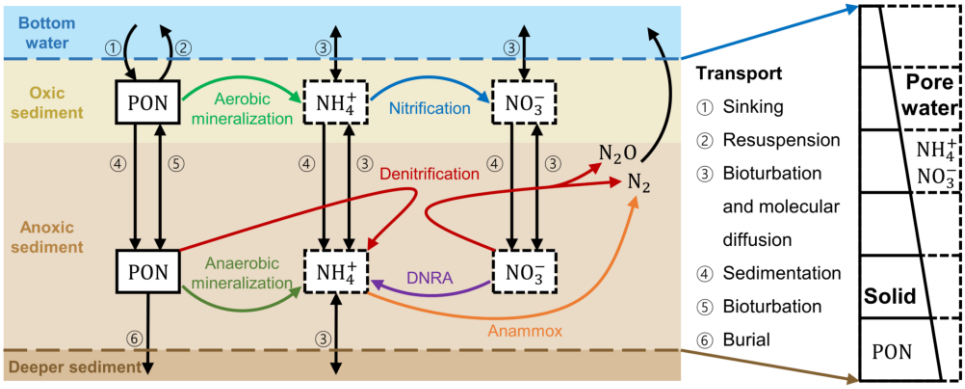

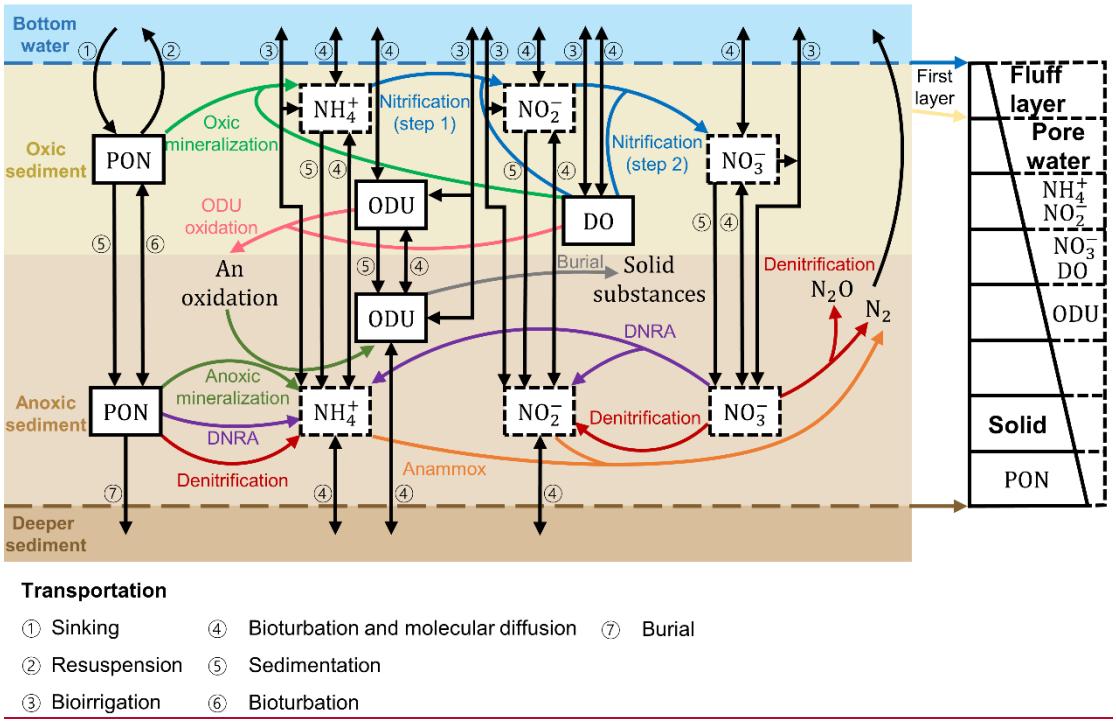

Figure ~~1~~2. Physical and biogeochemical processes for nitrogen cycle in the sediment model. ~~Three~~Six state variables in the model are PON, $\mathbf{NH_4^+}$ ~~and~~, $\mathbf{NO_2^-}$, $\mathbf{NO_3^-}$~~,~~, DO and ODU (the oxygen demand units). PON is a solid substance (enclosed by solid lines), while $\mathbf{NH_4^+}$ ~~and~~, $\mathbf{NO_2^-}$, $\mathbf{NO_3^-}$, DO and ODU are dissolved substances in the pore water (enclosed by dash lines). The physical processes and biogeochemical processes are denoted by black arrows and coloured arrows, respectively. The numbers with circle denote the transport processes included in the model.

In the solid part, the fast-decayed and slow-decayed PON are treated with a large and small mineralization rate, respectively. Both of them undergo identical vertical transport processes, including downward sedimentation driven by gravity and vertical diffusion caused by bioturbation. Their mineralization occurring within the sediment provides a flux of NH_4^+ into the pore water.

In the pore water, the dissolved NH_4^+ ~~and~~, NO_2^-, NO_3^-, DO and ODU are transported downward and diffused vertically, as corresponding to both bioturbation and molecular diffusion. The biogeochemical processes occurring within the pore water include nitrification, denitrification, anammox~~ and~~, dissimilatory nitrate reduction to ammonium (DNRA~~).~~), ODU oxidation and ODU burial.

At the sediment-water interface, the exchange of solid matter is controlled by the bottom shear stress. The solid matter in the water column sinks into the fluff layer when the bottom stress is below a critical value, while resuspension occurs when the bottom stress exceeds this threshold. The exchange fluxes of NH_4^+ ~~and~~, NO_2^-, NO_3^-, DO and ODU at the interface are determined by the product of the diffusion coefficient and their concentration gradient between the fluff layer and the overlying water.

In the deepest layer of sediment, only the slow-decayed PON is allowed to move downward and leave the model domain via burial. The exchange fluxes of NH_4^+, NO_2^- and ODU between the model domain and the underlying pore water ~~is~~are calculated by the production of the diffusion coefficient and the concentration gradient derived from the model results at the nearest grid point and the observations in the underlying pore water, while the exchange fluxes of NO_3^- and DO there ~~is~~are set to zero.

2.~~2~~3 Equations and parameters

The equations for the concentrations of solid matter (C_s, $mmol\ m^{-3}$) and dissolved matter (C_d, $mmol\ m^{-3}$) are as follows:

$$\frac{\partial[(1-\emptyset)\cdot C_s]}{\partial t} = \frac{\partial[(1-\emptyset)\cdot D_B\cdot\frac{\partial C_s}{\partial z}]}{\partial z} - \frac{\partial[\omega\cdot(1-\emptyset)\cdot C_s]}{\partial z} + (1-\emptyset)\cdot\sum R_s \quad (1)$$

$$\frac{\partial[\emptyset\cdot C_d]}{\partial t} = \frac{\partial[\emptyset\cdot(D_B+D_M)\cdot\frac{\partial C_d}{\partial z}]}{\partial z} - \frac{\partial[\omega\cdot\emptyset\cdot C_d]}{\partial z} + \emptyset\cdot\sum R_d + \emptyset\cdot\alpha\cdot(C_d^w - C_d) + \emptyset\cdot\sum R_d \quad (2)$$

Where z (m) is vertical axis for sediment depth, t (s) is time, $\emptyset$ is the sediment porosity, D_B ~~and D_M~~ are($m^2\ s^{-1}$) is the bioturbation coefficient ~~and~~ , D_M ($m^2\ s^{-1}$) is the molecular diffusion coefficient ~~($m^2\ s^{-1}$),~~ ω ($m\ s^{-1}$) is the sedimentation ~~rate ($mm\ yr^{-1}$),~~velocity, α (s^{-1}) is the bioirrigation coefficient, C_d^w ($mmol\ m^{-3}$) is the concentration of dissolved matter in the bottom water, R_s is the biochemical reaction rate of PON, and R_d is the biochemical reaction rate of dissolved matter, including NH_4^+ ~~and~~, NO_2^-, NO_3^-~~,~~ DO and ODU. Since the sediment type in the study area is muddy, the advection of pore water in sandy sediments controlled by pressure is neglected.

The vertical profile of D_B is expressed as equation (3) (Radtke et al., 2019).

$$D_B(z) = \begin{cases} D_{B_{max}}, & 0 < z < z_{max} \\ D_{B_{max}}\cdot\exp\left(-\frac{z-z_{max}}{z_d}\right), & z \geq z_{max} \end{cases} \quad (3)$$

Where z_{max} (m) is the depth down to which the maximum bioturbation coefficient ($D_{B_{max}}$) is applied, z_d (m) is the decaying length scale of $D_{B_{max}}$~~.~~ ($m^2\ s^{-1}$).

D_M of dissolved matter in the pore water is a function of porosity, and is expressed as follows (Boudreau et al., 1998; Radtke et al., 2019):

$$D_M(z) = \frac{D_\sigma}{1-2.02\ln(\emptyset)} = \frac{D^T}{1-2.02\ln(\emptyset)} \quad (4)$$

where ~~D_0~~ D^T ~~$(m^2\ s^{-1})$~~ is the diffusion coefficient of the dissolved matter in the particle-free liquid ~~$(m^2\ s^{-1})$.~~ at T °C. The relationship between D^T and temperature (T) is expressed as (Soetaert et al., 1996):

$$D^T = D_0 + a \cdot T \quad (5)$$

where D_0 $(m^2\ s^{-1})$ is the diffusion coefficient of the dissolved matter in the particle-free liquid at 0 °C, a $(m^2\ s^{-1}\ (°C)^{-1})$ is an ion-specific coefficient.

Bioirrigation characterizes the dissolved matter exchange caused by biological burrowing activities, and the coefficient decreases with depth (Dale et al., 2011):

$$\alpha(z) = \alpha_1 \cdot \frac{\exp(\alpha_2 - z)}{1+\exp(\alpha_2 - z)} \quad (6)$$

The parameters α_1 (s^{-1}) and α_2 (m) represent the magnitude of bioirrigation and the depth at which it decreases to half of α_1, respectively.

The biochemical reactions are expressed in equations (~~5)~~ ~~(~~7)-(12). Detailed descriptions of these reactions are presented in Table 1 (Soetaert et al., 1996; Capet et al., 2016; Akbarzadeh et al., 2018). These reaction equations primarily consider the limitations imposed by DO and temperature on each reaction. ~~Due to the lack of parameterization schemes, it is difficult to represent the competition between different organisms for the same reaction. Since this is not the focus of this paper, we describe them collectively as a unified, generalized concept based on reaction rates.~~ All the related coefficients and parameters are listed in Table 2. The sensitivity analysis of the model parameters is shown in Figure S3 and Text S1.

$$\sum R_{PON} = -\frac{O_2}{K_{min}} R_{Min}^{OM} - \frac{K_{den}}{K_{min}} R_{Den} - \frac{NO_3}{K_{min}} R_{Min}^{AM} - R_{DNRA} \quad (~~5~~7)$$

$$\sum R_{NH_4^+} = \frac{O_2}{K_{min}} R_{Min}^{OM} + \frac{K_{den}}{K_{min}} R_{Den} + \frac{NO_3}{K_{min}} R_{Min}^{AM} - R_{Nit1} + (1 + 0.5 \cdot r_{C:N}(1-\delta) \cdot r_{C:N}) R_{DNRA} - R_{nit} - R_{Ana} \quad (~~6~~8)$$

$$\sum R_{NO_2^-} = 0.8 \cdot \alpha \cdot r_{C:N} \cdot R_{den} + R_{Nit1} - R_{Nit2} + 0.5 \cdot \delta \cdot r_{C:N} \cdot R_{DNRA} - R_{Ana} \quad (9)$$

$$\sum R_{NO_3^-} = R_{nit} = R_{Nit2} - 0.8 \cdot r_{C:N} \cdot R_{den} - 0.5 \cdot r_{C:N} \cdot R_{DNRA} - 0.8 \cdot r_{C:N} \cdot R_{den} \quad (~~7~~10)$$

$$\sum R_{O_2} = -r_{C:N} \cdot R_{Min}^{OM} - 1.5 \cdot R_{Nit1} - 0.5 \cdot R_{Nit2} - R_{ODUox} \quad (11)$$

$$\sum R_{ODU} = r_{C:N} \cdot (1 - r_{ODUsolid}) \cdot R_{Min}^{AM} - R_{ODUox} \quad (12)$$

227 Table 1. Reaction formulas and rate expressions.

Process	Formula	Rate expression
~~Aerobic~~Oxic mineralization_ (R_{Min}^{OM})	$(CH_2O)_x(NH_3)_y$~~$(H_3PO_4)_z + xO_2$~~ ~~$\rightarrow yNH_4^+ + xH_z$~~ $+ xO_2$ $\rightarrow yNH_4^+ + (x-y)CO_2$ $+ yHCO_3^- + (x-y)H_2O$	~~$R_{min}^{O_2}$~~R_{Min}^{OM} $= r_{min} \cdot PON \cdot Q^{\frac{T-20}{10}}$ $\cdot \frac{~~O_2~~}{~~O_2 + Ks_{O_2}~~} \frac{O_2}{O_2 + Ks_{O_2}^{OM}}$ $\cdot \frac{1}{\sum lim}$
Denitrification_ (R_{Den})	$(CH_2O)_x(NH_3)_y$~~$(H_3PO_4)_z$~~ $+ 0.8xNO_3^-$ $\rightarrow yNH_4^+ + 0.$~~$4x(1 - \alpha)N_z$~~$8\alpha xNO_2^-$ $+ 0.4(1-\alpha-\beta)xN_2$ $+ 0.$~~$4x\alpha$~~$4\beta xN_2O$ $+$ ~~$1.4xH_zO$~~$(0.2x - y + 0.8\alpha x)CO_2$ $+ (0.8x - 0.8\alpha x + y)HCO_3^-$ $+ (0.6x - y - 0.8\alpha x - 0.4\beta x)H_2O + (0.8\alpha x - 0.4\beta x)H_2$	~~R_{den}~~R_{Den} $= r_{min} \cdot PON \cdot Q^{\frac{T-20}{10}}$ $\cdot \frac{~~NO_3^-~~}{~~NO_3^- + Ks_{NO_3^-}~~}$ $\cdot \left(1 - \frac{~~O_2~~}{~~O_2 + Kin_{O_2}^{Den}~~}\right)$ $\cdot \frac{~~1~~}{~~\sum lim~~} \frac{NO_3^-}{NO_3^- + Ks_{NO_3^-}^{Den}}$ $\cdot \frac{Kin_{O_2}^{Den}}{O_2 + Kin_{O_2}^{Den}} \cdot \frac{1}{\sum lim} \cdot \gamma$
An~~aer~~o~~b~~xic mineralization_ (R_{Min}^{AM})	$(CH_2O)_x(NH_3)_y$~~$(H_3PO_4)_z$~~ + an oxidant $\rightarrow yNH_4^+ + xCO_2 + xODU + xH_2O$	~~R_{min}^{AM}~~R_{Min}^{AM} $= r_{min} \cdot PON \cdot Q^{\frac{T-20}{10}}$ $\cdot \left(1 - \frac{~~O_2~~}{~~O_2 + Kin_{O_2}^{AM}~~}\right)$ $\cdot \left(1 - \frac{~~NO_3^-~~}{~~NO_3^- + Kin_{NO_3^-}~~}\right)$ $\cdot \frac{Kin_{O_2}^{AM}}{O_2 + Kin_{O_2}^{AM}}$ $\cdot \frac{Kin_{NO_3^-}^{AM}}{NO_3^- + Kin_{NO_3^-}^{AM}} \cdot \frac{1}{\sum lim}$

Nitrification_step1 (R_{Nit1})	$NH_4^+ + 1.5O_2 + 2HCO_3^- \rightarrow NO_2^- + 3H_2O + 2CO_2$	$R_{Nit1} = r_{nit1} \cdot \frac{NH_4^+}{NH_4^+ + Ks_{NH_4^+}^{Nit1}} \cdot \frac{O_2}{O_2 + Ks_{O_2}^{Nit1}}$
Nitrification_step2 (R_{Nit2})	$NO_2^- + 0.5\cancel{NH_4^+ + 2}O_2 \rightarrow NO_3^- \cancel{+ H_2O}$	$\cancel{R_{nit} = r_{nit} \cdot NH_4^+ \cdot \frac{O_2}{O_2 + Ks_{Nit}}} R_{Nit2} = r_{nit2} \cdot \frac{NO_2^-}{NO_2^- + Ks_{NO_2^-}^{Nit2}} \cdot \frac{O_2}{O_2 + Ks_{O_2}^{Nit2}}$
DNRA (R_{DNRA})	$(CH_2O)_x(NH_3)_y\cancel{(H_3PO_4)_z} + 0.5xNO_3^- + (1-\delta)xH^+ \rightarrow \cancel{(0.5x+y)}(0.5(1-\delta)x + y)NH_4^+ + 0.5\delta xNO_2^- + yHCO_3^- + (x-y)CO_2 + (0.5x - y - \delta x)H_2O + 1.5\delta xH_2$	$R_{DNRA} = r_{min} \cdot PON \cdot Q^{\frac{T-20}{10}} \cdot \frac{\cancel{NO_3^-}}{\cancel{NO_3^- + Ks_{NO_3^-}}} \cdot \left(1 - \frac{\cancel{O_2}}{\cancel{O_2 + Kin_{O_2}^{Den}}}\right) \cdot \frac{\cancel{1}}{\cancel{\sum lim}} \frac{NO_3^-}{NO_3^- + Ks_{NO_3^-}^{Den}} \cdot \frac{Kin_{O_2}^{Den}}{O_2 + Kin_{O_2}^{Den}} \cdot \frac{1}{\sum lim} \cdot (1-\gamma)$
Anammox (R_{Ana})	$NH_4^+ + NO_2^- \rightarrow N_2 + 2H_2O$	$\cancel{R_{Ana} = r_{Ana} \cdot \frac{NH_4^+}{NH_4^+ + Ks_{NH_4^+}} \cdot \frac{NO_2^-}{NO_2^- + Ks_{NO_2^-}} \cdot \frac{Kin_{O_2}^{Ana}}{O_2 + Kin_{O_2}^{Ana}}} R_{Ana} = r_{Ana} \cdot \frac{NH_4^+}{NH_4^+ + Ks_{NH_4^+}^{Ana}} \cdot \frac{NO_2^-}{NO_2^- + Ks_{NO_2^-}^{Ana}} \cdot \frac{Kin_{O_2}^{Ana}}{O_2 + Kin_{O_2}^{Ana}}$

	ODU oxidation (R_{ODUox})	$ODU + O_2 \rightarrow$ an oxidant	$R_{ODUox} = r_{ODUox} \cdot ODU \cdot \frac{O_2}{O_2 + Ks_{O_2}^{ODUox}}$

228 $\sum \lim = \frac{\cancel{O_2}}{\cancel{O_2}+\cancel{Ks_{O_2}}} \frac{O_2}{O_2+Ks_{O_2}^{OM}} + \frac{\cancel{NO_3^-}}{\cancel{NO_3^-}+\cancel{Ks_{NO_3^-}}} \cdot \left(1-\frac{\cancel{O_2}}{\cancel{O_2}+Kin_{\cancel{O_2}}^{Den}}\right) + \left(1-\frac{\cancel{O_2}}{\cancel{O_2}+Kin_{\cancel{O_2}}^{AM}}\right) \cdot \left(1-\right.$

229 $\left.\frac{\cancel{NO_3^-}}{\cancel{NO_3^-}+\cancel{Kin_{NO_3^-}}}\right) \cdot \frac{NO_3^-}{NO_3^-+Ks_{NO_3^-}^{Den}} \cdot \frac{Kin_{O_2}^{Den}}{O_2+Kin_{O_2}^{Den}} + \frac{Kin_{O_2}^{AM}}{O_2+Kin_{O_2}^{AM}} \cdot \frac{Kin_{NO_3^-}^{AM}}{NO_3^-+Kin_{NO_3^-}^{AM}}$. x: y: ~~z~~ = C: N: ~~P.~~

230

Table 2. Model parameters. (L: based on literature; M: constrained with the model, I: independently determined from observations).

Parameter	Value	Unit	Description	References
ω	2.68.24×10^{-11}	mm yrm s^{-1}	Sedimentation ratevelocity	(Ichimi et al., 2005)L[a]
$D_{B_{max}}$	1.152×10^{-11}	m^2 s^{-1}	Maximum bioturbation coefficient	(Soetaert et al., 1996)M
z_{max}	0.0105	m	Depth down to which the Mmaximum bioturbation coefficient is applied	(Soetaert et al., 1996)L[b]
z_d	0.505	m	Decaying length scale of the maximum bioturbation coefficient	(Soetaert et al., 1996)L[b, d]
$D_0^{NH_4^+}$	0.8479.80×10^{-10}	cm^2 dm^2 s^{-1}	The molecular diffusion coefficient of ammonium NH_4^+ in a particle-free solution at 0 °C	(Soetaert et al., 1996)L[b]
$D_0^{NO_2^-}$	9.16×10^{-10}	m^2 s^{-1}	The molecular diffusion coefficient of NO_2^- in a particle-free solution at 0 °C	L[c]
$D_0^{NO_3^-}$	0.8459.78×10^{-10}	cm^2 dm^2 s^{-1}	The molecular diffusion coefficient of nitrate NO_3^- in a particle-free solution at 0 °C	(Soetaert et al., 1996)L[b]

D_0^{DO}	1.11×10^{-9}	$m^2\ s^{-1}$	The molecular diffusion coefficient of DO (dissolved oxygen) in a particle-free solution at 0 ℃	L[b]
D_0^{ODU}	9.74×10^{-10}	$m^2\ s^{-1}$	The molecular diffusion coefficient of ODU (the oxygen demand units) in a particle-free solution at 0 ℃	L[b]
$a_{NH_4^+}$	3.89×10^{-11}	$m^2\ s^{-1}\ (℃)^{-1}$	Coefficient for temperature dependency of diffusion coefficient of NH_4^+	L[b]
$a_{NO_2^-}$	3.89×10^{-11}	$m^2\ s^{-1}\ (℃)^{-1}$	Coefficient for temperature dependency of diffusion coefficient of NO_2^-	L[b]
$a_{NO_3^-}$	3.89×10^{-11}	$m^2\ s^{-1}\ (℃)^{-1}$	Coefficient for temperature dependency of diffusion coefficient of NO_3^-	L[b]
a_{DO}	4.47×10^{-11}	$m^2\ s^{-1}\ (℃)^{-1}$	Coefficient for temperature dependency of diffusion coefficient of DO	L[b]

a_{ODU}	2.80×10^{-11}	m^2 s^{-1} $(℃)^{-1}$	Coefficient for temperature dependency of diffusion coefficient of ODU	L[b]
α_1	1.16×10^{-7}	s^{-1}	The magnitude of bioirrigation	M
α_2	0.09	m	the depth at which bioirrigation coefficient decreases to half of α_1	L[d]
r_{minf}	~~2.8~~3×10^{-9}~~8~~	s^{-1}	Mineralization ~~rate~~coefficient of fast decay organic nitrogen	M
r_{mins}	~~1.05~~7×10^{-9}~~10~~	s^{-1}	Mineralization ~~rate~~coefficient of slow decay organic nitrogen	M
Q	2		Factor for temperature effect on mineralization	~~(Capet et al., 2016)~~L[e]
~~Ks_{O_2}~~$Ks_{O_2}^{OM}$	3	~~μmol L^{-1}~~mmol m^{-3}	Half saturation constant of ~~oxygen~~DO in ~~aer~~o~~b~~x~~i~~c mineralization	~~(Soetaert et al., 1996)~~L[b]
~~$Ks_{NO_3^-}$~~$Ks_{NO_3^-}^{Den}$	30	~~μmol L^{-1}~~mmol m^{-3}	Half saturation constant of ~~nitrate~~NO_3^- in denitrification	~~(Soetaert et al., 1996)~~L[b]

$Kin_{O_2}^{Den}$	10	~~μmol L^{-1}~~mmol m^{-3}	Half saturation constant of ~~oxygen~~DO in denitrification	~~(Soetaert et al., 1996)~~L[b]
α	5	%	Nitrite leakage during denitrification	L[c]
β	1	%	Nitrous oxide leakage during denitrification	L[c]
γ	95	%	Fraction of total ~~nitrate~~ NO_3^- Reduction occurring via denitrification	~~(Akbarzadeh et al., 2018)~~L[c]
$Kin_{O_2}^{AM}$	5	mmol m^{-3}~~μmol L^{-1}~~	Half saturation constant of ~~oxygen~~DO in an~~aer~~o~~b~~xic mineralization	~~(Soetaert et al., 1996)~~L[b]
~~$Kin_{NO_3^-}$~~$Kin_{NO_3^-}^{AM}$	5	~~μmol L^{-1}~~mmol m^{-3}	Half saturation constant of ~~nitrate~~ NO_3^- in an~~aer~~o~~b~~xic mineralization	~~(Soetaert et al., 1996)~~L[b]
~~r_{nit}~~r_{nit1}	~~2~~1.16×10^{-4}	~~d~~mmol m^{-3} s^{-1}	Maximum coefficient of nitrification ~~rate~~(step 1)	~~(Soetaert et al., 1996)~~M
r_{nit2}	1.16×10^{-3}	mmol m^{-3} s^{-1}	Maximum coefficient of nitrification (step 2)	M

~~Ks_{nit}~~$Ks_{NH_4^+}^{Nit1}$	~~1~~10	mmol m~~$^{-3}$~~ ~~μmol L^{-1}~~	Half saturation constant of ~~oxygen~~ NH_4^+ in nitrification (step 1)	~~(Soetaert et al., 1996)~~L[c]
$Ks_{O_2}^{Nit1}$	15.6	mmol m^{-3}	Half saturation constant of DO in nitrification (step 1)	L[c]
$Ks_{NO_2^-}^{Nit2}$	10	mmol m^{-3}	Half saturation constant of NO_2^- in nitrification (step 2)	L[c]
$Ks_{O_2}^{Nit2}$	34.4	mmol m^{-3}	Half saturation constant of DO in nitrification (step 2)	L[c]
δ	5	%	Nitrite leakage during DNRA	L[c]
r_{Ana}	2.~~3~~31×10^{-4}~~5~~	mmol m^{-3} s^{-1}	Maximum anammox ~~rate~~coefficient	~~(Akbarzadeh et al., 2018)~~M
~~$Ks_{NH_4^+}$~~$Ks_{NH_4^+}^{Ana}$	5	~~μmol L^{-1}~~mmol m^{-3}	Half saturation constant of ~~ammonium~~NH_4^+ in anammox	~~(Akbarzadeh et al., 2018)~~L[c]
~~$Ks_{NO_2^-}$~~$Ks_{NO_2^-}^{Ana}$	5	~~μmol L^{-1}~~mmol m^{-3}	Half saturation constant of ~~nitrite~~NO_2^- in anammox	~~(Akbarzadeh et al., 2018)~~L[c]
$Kin_{O_2}^{Ana}$	8	~~μmol L^{-1}~~mmol m^{-3}	Half saturation constant of ~~oxygen~~DO in anammox	~~(Akbarzadeh et al., 2018)~~L[c]

r_{ODUox}	1.16×10^{-5}	s^{-1}	Maximum ODU oxidation coefficient	L[f]
$Ks_{O_2}^{ODUox}$	1	mmol m^{-3}	Half saturation constant of DO in ODU oxidation	L[b]
$r_{ODUsolid}$	0.99	s^{-1}	Part of ODU production that is deposited as a solid	L[g]
$r_{C:N}$	10.2		Ratio of carbon to nitrogen	I
~~α~~	~~1~~	~~%~~	~~Nitrous oxide leakage during denitrification~~	~~(Akbarzadeh et al., 2018)~~
w	2.31×10^{-5}	m s^{-1}	Sinking ~~rate~~velocity	~~(Ding et al., 2020)~~L[h]
τ_c	0.06	N m^{-2}	Critical bottom stress	~~(Ding et al., 2020)~~M
E_{PON}	1×10^{-8}	mmol m^{-2} s^{-1}	Resuspension coefficient	~~(Ding et al., 2020)~~L[h]
D_{sur}	~~7~~1×10$^{-~~7~~9}$	m^2 s^{-1}	Surface diffusion coefficient	~~(Radtke et al., 2019)~~M
Δz	3×10^{-3}	m	Distance of the diffusion layer at sediment-water interface	~~(Nakakuni et al., 2024)~~L[i]

[a] Ichimi et al. (2005)

[b] Soetaert et al. (1996)

[c] Akbarzadeh et al. (2018)

[d] Dale et al. (2011)

[e] Capet et al. (2016)

[f] Laurent et al. (2016)

[g] Pastor et al. (2011)

[h] Ding et al. (2020)

[i] Wang et al. (2016)

Due to the large biomass of benthos and ~~high DO concentrations~~the characteristics of rapid change in the fluff layer, the mineralization ~~rate~~coefficient in this layer is set to be 50 times faster than that in the sediment below it (Lee et al., 2002; Kuhrts et al., 2006; Laima et al., 2002).

At the sediment-water interface, the sinking and resuspension of PON depend on the bottom stress. The exchange flux (F_s) is expressed as (Wang, 2002):

$$F_s = \begin{cases} w \cdot C_s^w \cdot (\frac{\tau}{\tau_c} - 1), & \tau < \tau_c \\ E_s \cdot (\frac{\tau}{\tau_c} - 1), & \tau \geq \tau_c \end{cases} \quad (~~8~~13)$$

where w ($m\ s^{-1}$) is the sinking velocity of particles in the bottom water ~~($m\ s^{-1}$),~~ C_s^w ($mmol\ m^{-3}$) is concentration of PON in the bottom water ~~($mmol\ m^{-3}$),~~ τ ($N\ m^{-2}$) is the bottom stress ~~($N\ m^{-2}$),~~ τ_c ($N\ m^{-2}$) is the critical bottom stress ~~($N\ m^{-2}$),~~ E_s ($mmol\ m^{-2}\ s^{-1}$) is the resuspension ~~rate ($mmol\ m^{-2}\ s^{-1}$).~~coefficient.

The exchanges of dissolved matters (NH_4^+ ~~and~~, NO_2^-, NO_3^-~~)~~, DO and ODU) are mainly through bioturbation, bioirrigation and molecular diffusion, and the flux (F_d) is expressed as (Boudreau et al., 1998):

$$F_d = -D_{sur} \cdot \emptyset \cdot \frac{C_d^w - C_d^{pw}}{\Delta z} \quad (9$$

$$= -(D_{sur} + D_M^s) \cdot \emptyset \cdot \frac{C_d^w - C_d^{pw}}{\Delta z} \quad (14)$$

where D_{sur} ($m^2\ s^{-1}$) is the surface diffusion coefficient, D_M^s ($m^2\ s^{-1}$~~). C_d^w and~~) is the surface molecular coefficient, C_d^{pw} ~~are~~($mmol\ m^{-3}$) is the concentration~~s~~ of dissolved matter in the ~~bottom water and~~ pore water of fluff layer, ~~respectively ($mmol\ m^{-3}$). Δz~~Δz (m) is the distance of the diffusion layer at sediment-water interface ~~(m).~~.

At the bottom of the model domain, the slow-decayed PON is allowed to move out as the burial process with a flux (B_s) as (Radtke et al., 2019):

$$B_s = \omega \cdot (1 - \emptyset) \cdot C_s^b \quad (~~10~~15)$$

where superscript of b represents the deepest layer of the model domain.

The bottom ~~flux~~ fluxes (B_d) of NH_4^+ ~~(B_d) is,~~ NO_2^- and ODU are expressed as:

$$B_d = -(D_B^b + D_M^b) \cdot \emptyset \cdot \frac{C_d^b - C_d^{bc}}{\Delta z^b} \quad (~~11~~16)$$

where C_d^{bc} is NH_4^+ concentration in the pore water under the deepest layer of the model domain ($mmol\ m^{-3}$~~).~~), whose values are given from observations.

2.3 Study area

Harima Nada is situated within Seto Inland Sea, the largest semi-enclosed sea in Japan (Figure 2). It has an average water depth of 26 meters and is connected to Osaka Bay and Hiuchi Nada on the eastern and western sides, respectively. To the south, it connects to the Pacific Ocean through the Naruto Strait and Kii Channel (Zhu et al., 2019; Chang et al., 2009). Over the past few decades, the environment of the Seto Inland Sea has undergone significant changes (Ishii et al., 2014; Yamamoto et al., 2021). With the continuous observations of sediments in Harima Nada by our collaborators, we have realized that the DIN input from sediments in this area is comparable to that from rivers, exhibiting notable seasonal variations (Leng et al., 2023; Nakakuni et al., 2024). However, the driving factors and mechanisms behind these seasonal changes remain unclear. Therefore, Harima Nada serves as an excellent study area, and these observational data can provide a sufficient validation to ensure the reliability of model results (Nakakuni et al., 2024). This allows us to analyze the seasonal variations in sediment nitrogen cycling and interfacial nitrogen fluxes, as well as their controlling mechanisms. Additionally, this study lays the groundwork for future exploration of how sediment nitrogen cycling responds to long-term changes in the aquatic environment.

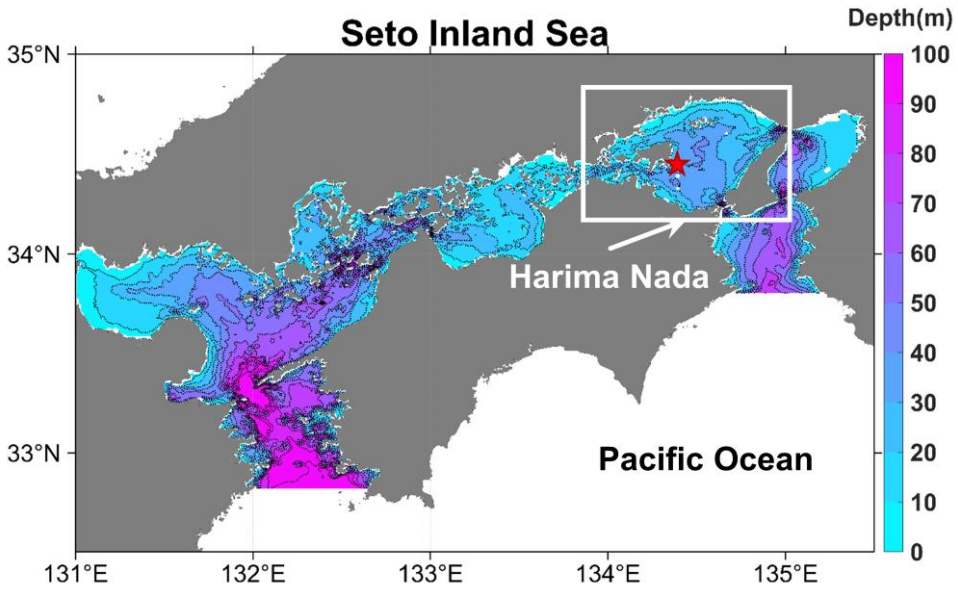

Figure 2. Study area of the Harima Nada, Japan. The red star represents the site where the observational data used in this study were collected.

2.4 Model configurations

Since this study focuses on seasonal changes at the sediment–water interface, the sediment depth in the model was set to 10 cm and uniformly divided into 100 layers.

The initial ~~concentrations of the four state variables were~~ sediment concentration profile of PON was obtained from ~~the~~ core observations in Harima Nada in July 2020, while those of NH_4^+, NO_2^- and NO_3^- were derived from observations conducted in April (Nakakuni et al., 2024). ~~Moreover, the observed profile of DO concentration~~ The DO profile was adopted from previous observations in the Seto Inland Sea (Sayama et al., 2002~~), nitrite (NO_2^-)~~). The ODU concentration~~, and~~ was initially set to 100 mmol m^{-3} and allowed to evolve dynamically within the model. In addition, the porosity ~~were also included and always~~profile was prescribed as a constant ~~in the model as~~ input condition throughout the simulation (Figure ~~S2c e~~S4 and Text S2).

Monthly observations of bottom water temperature and concentrations of ~~PON,~~ NH_4^+, NO_x^- ($NO_2^- + NO_3^-$) and ~~NO_3^-~~DO from ~~February~~April 2020 to ~~January~~April 2021 were used to prescribe the upper boundary conditions, while NH_4^+ and NO_2^- concentration beneath the model domain from April 2020 to May 2021 served as the bottom boundary conditions (Nakakuni et al., 2024). The concentration of PON and NO_2^- in the bottom water were collected from the seasonal dataset of Japanese Ministry of the Environment from January 2020 to May 2021.~~2024).~~ The bottom stress was derived from a hydrodynamic model for the Seto Inland Sea (Zhu et al., 2019) (Figure 3). The ODU concentration in the bottom water was set to 0 mmol m^{-3}, while its concentration in the deeper sediment was assumed to be the initial value of 100 mmol m^{-3} (Soetaert et al., 1996). Forced by these boundary conditions, the sediment model simulated the nitrogen cycle changes in the sediments of Harima Nada from April 2020 to March 2021. And it was calculated for a long time (more than ~~500~~170 years) to reach a steady-state condition, wherein the input and output fluxes of materials become balanced.

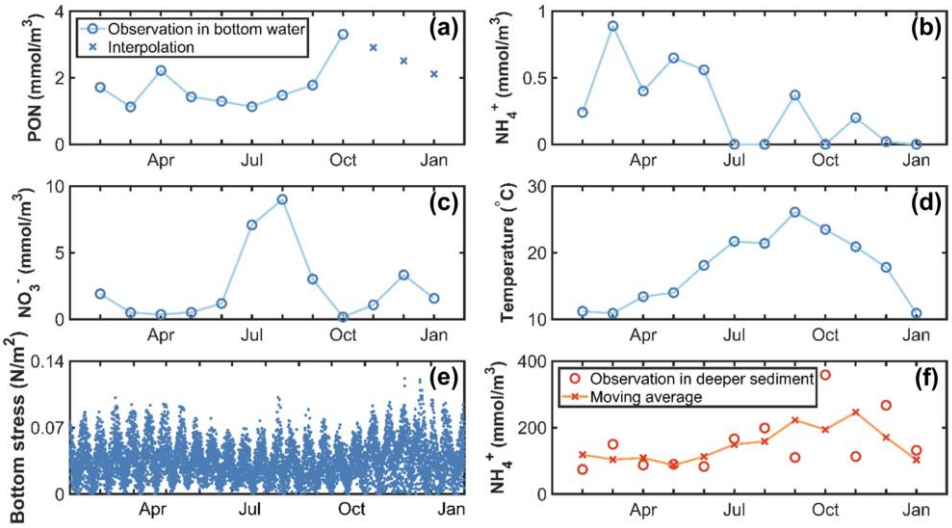

311

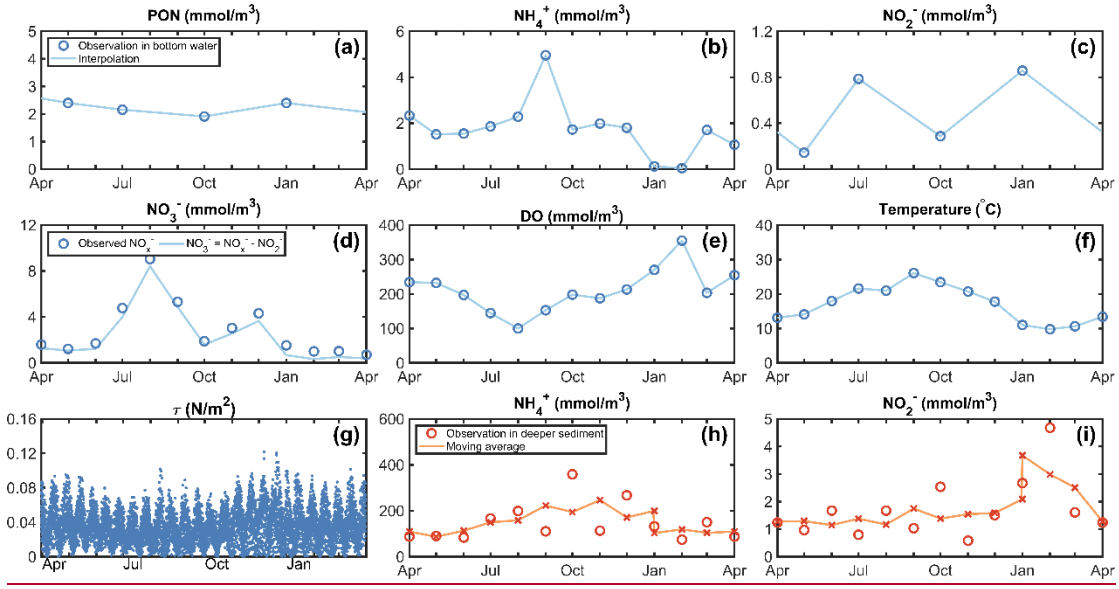

312

313 **Figure 3.** ~~Boundary~~Model boundary conditions ~~of~~for the ~~model~~simulation period spanning April 2020 to March
314 2021: (a) PON concentration, (b) $\mathbf{NH_4^+}$ concentration, (c) $\mathbf{NO_2^-}$ concentration, (d) $\mathbf{NO_3^-}$ concentration, (e) DO
315 concentration in the bottom water, (~~d~~f) bottom water temperature, (~~e~~g) bottom stress ~~and (f,~~ (h) $\mathbf{NH_4^+}$ concentration
316 and (c) $\mathbf{NO_2^-}$ concentration in the layer below model domain (10-12 cm). ~~The~~The extrapolation shown in panels (a)
317 and (c) utilizes the observed values ~~of PON concentration in the bottom water~~ from ~~November to~~ January ~~are~~
318 ~~obtained by linear~~2020 and May 2021 for interpolation~~. A~~, which are not displayed in this figure. For panels (h) and
319 (i), monthly observations are smoothed using a three-point moving average ~~is applied~~ to ~~$\mathbf{NH_4^+}$ concentrations in (f)~~
320 ~~to smooth out~~reduce intra-seasonal ~~fluctuations~~variability.

321

3 Results

3.1 Seasonal variations of the particle and dissolved nitrogen concentrations in the sediment

The monthly concentrations of PON, NH_4^+, DO, NO_2^- and NO_3^- at different layers from 0 to 10 cm in the model domain are shown in Figure 4, alongside the corresponding observed data. The comparison between the model results and the observations, especially ~~for the data in July (Figure 4d-e),~~the seasonal variations, suggests a reliable performance of the model.

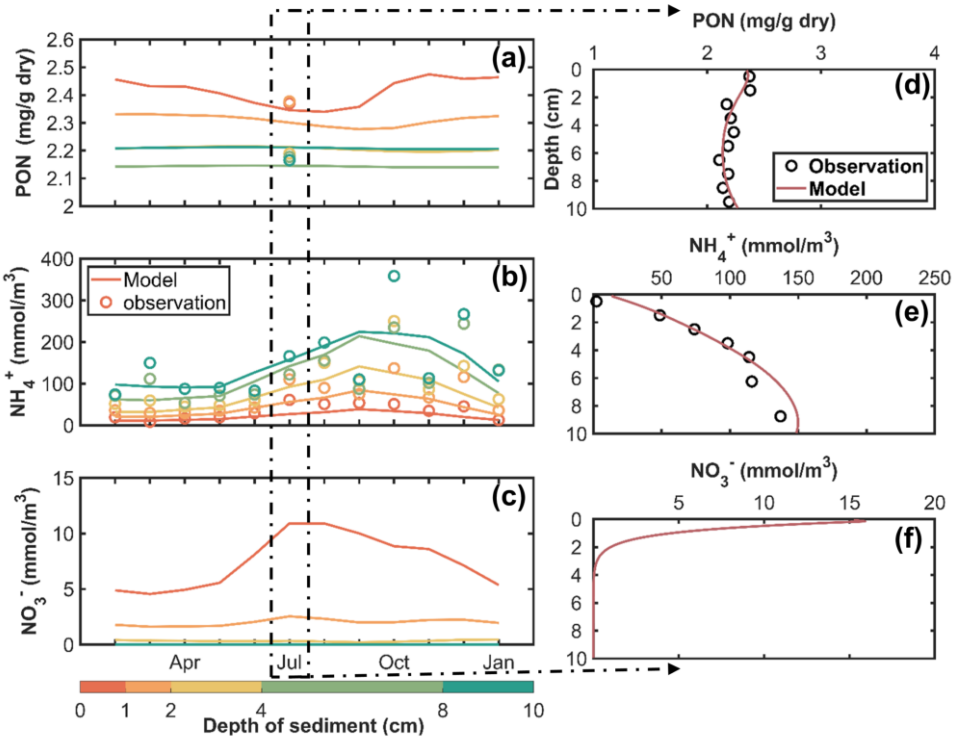

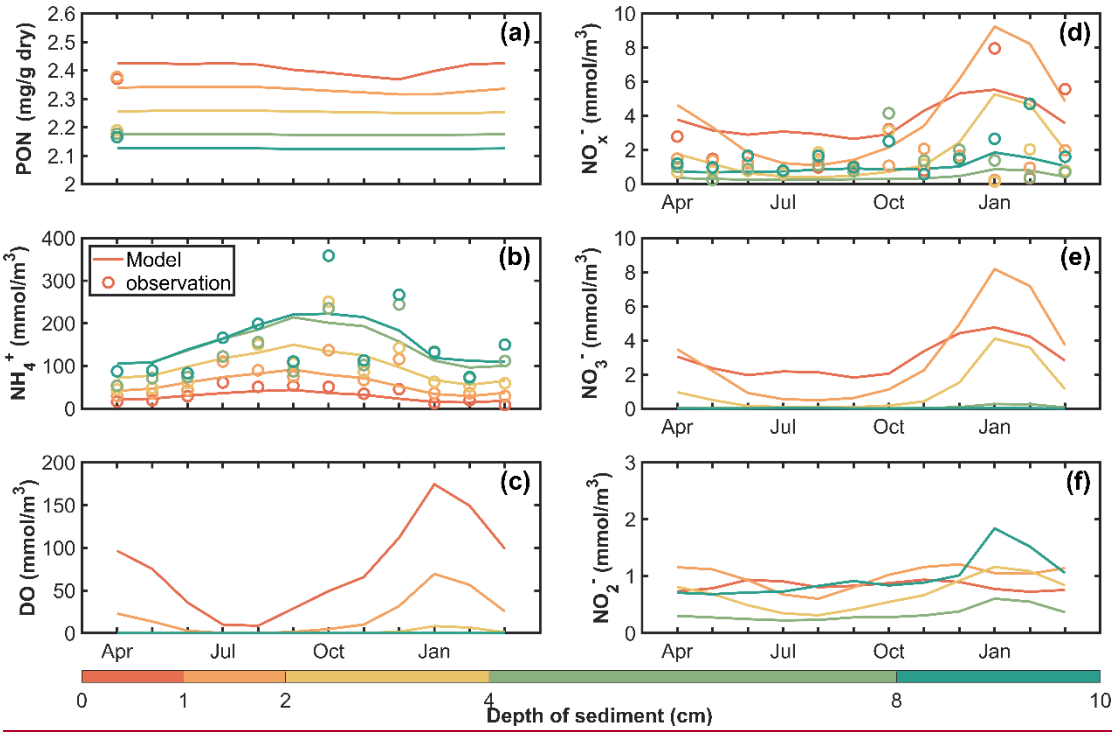

Figure 4. The seasonal variations of concentrations of (a) PON, (b) $\mathbf{NH_4^+}$ ~~and~~, (c) ~~$\mathbf{NO_3^-}$~~DO, (d) $\mathbf{NO_x^-}$ ~~($\mathbf{NO_2^-}$ + $\mathbf{NO_3^-}$)~~, (e) $\mathbf{NO_3^-}$ and (f) $\mathbf{NO_2^-}$ in different layers in the sediment~~, the vertical profiles of (d) PON, (e) $\mathbf{NH_4^+}$ and (f) $\mathbf{NO_3^-}$ in July. Colors in (a)-(c)~~. Colours represent different depth. In all the panels, lines are model results and circles are the observation data.

The concentration of PON in the sediment was consistently greater in the surface layer compared to the underlying layers (Figure 4a). Its seasonal variation was apparent in the upper ~~3~~2 cm of sediment and almost disappears in the layers below ~~3~~2 cm. In the 0-1 cm layer, PON concentration decreased from a value of 2.~~46~~43 mg/g in ~~February~~April to a minimum value of 2.~~34~~37 mg/g in ~~August~~December, followed by an increase back to ~~a peak concentration of 2.47~~2.43 mg/g in ~~November~~March. In the deep layer of the sediment (8-10 cm), PON concentration remained around 2.~~20~~12 mg/g throughout the year. The NH_4^+concentration had a minimum value at the surface and a maximum value at the deepest layer (Figure 4b), which was contrary to the vertical distribution of PON concentrations. The NH_4^+ concentrations presented significant seasonal variations across entire sediment layers, with the range of variation increasing with depth. For example, the NH_4^+ concentration in the 0-1 cm layer presented the lowest value of ~~11.02~~14.65 mmol m^{-3} in February and the highest value of ~~38.71~~43.79 mmol m^{-3} in September; however, the NH_4^+ concentration in the deep layer of the sediment (8-10 cm) presented the lowest value of ~~90.97~~106.44 mmol m^{-3} in April and the highest value of ~~224.34~~222.35 mmol m^{-3} in ~~September~~October. Except for the episodic high values observed in the deep sediment layer during

autumn, the model successfully reproduced the seasonal variation of NH_4^+ concentration across all sediment layers, which was characterized by lower levels in winter and spring and elevated levels in summer and autumn.

~~NO_3^-~~The DO concentration ~~reached its peak~~ profiles exhibited a clear vertical gradient, with higher values at the ~~sediment~~ surface and ~~exhibited a rapid decline to zero~~ lower values in deeper layers (Figure 4c). Surface DO reach a maximum of 174.51 mmol m^{-3} in January and decreased to a minimum of 8.70 mmol m^{-3} in August. The oxygen penetration depth (OPD) remained below 1 cm from June to October, and extended below 2 cm only during January and February.

NO_3^- was the dominant component of NO_x^- (Figure 4d, e). From December to April, a subsurface maximum appeared at the ~~depth of around 3 cm (Figure 4c and f). Its seasonal variation~~layer of 1–2 cm, whereas during the rest of the year the highest concentrations occurred ~~within the upper 1 cm layer, showing a high~~at the surface layer. Within the 0–4 cm layer, NO_3^- exhibited a pronounced seasonal pattern, with lower concentrations in summer and higher concentrations in winter. Specifically, concentrations ranged from 1.82 to 4.76 mmol m^{-3} in the 0–1 cm layer, 0.49 to 8.18 mmol m^{-3} in the 1–2 cm layer, and 0.08 to 3.58 mmol m^{-3} in the 2–4 cm layer. Below 4 cm, NO_3^- concentrations remained close to zero throughout the year.

NO_2^- also showed the similar seasonal pattern, with lower concentrations in summer and higher concentrations in winter (Figure 4f). The maximum value ~~in summer. The~~ of 1.84 mmol m^{-3} occurred in January at the deepest layer. Vertically, NO_2^- maxima alternated between the 0–2 cm layer and the 8–10 cm layer. Notably, during January to February, the maximum concentration in the ~~0–1~~8–10 cm layer ~~was 10.91~~exceeded 1 mmol m^{-3}, whereas in ~~July, which was double~~other months the ~~minimum concentration of 4.56~~peak values remained around 1 mmol m^{-3} ~~in March.~~ .

3.2 The flux of PON, DIN and N-loss (N_2 and N_2O) between bottom water and sediment

In this section, we introduce the flux at the sediment-water interface, including the net sinking of PON and the exchange of dissolved substances caused by molecular diffusion and bioturbation, excluding bioirrigation. PON sank from the bottom water to the sediment throughout the year (Figure 5a). The PON flux ~~was high in fall~~exhibited a bimodal seasonal pattern, with ~~the maximum value of~~ two peaks in July

(2.9014 mmol m^{-2} d^{-1} ~~in October and low in spring with the minimum value of~~) and February (1.0796 mmol m^{-2} d^{-1} ~~in May.~~), and a minimum in November (1.50 mmol m^{-2} d^{-1}).

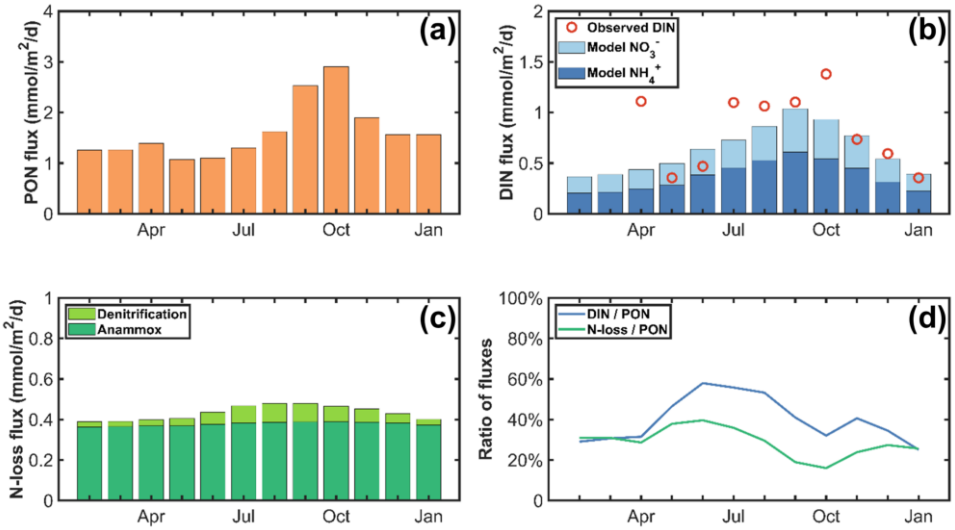

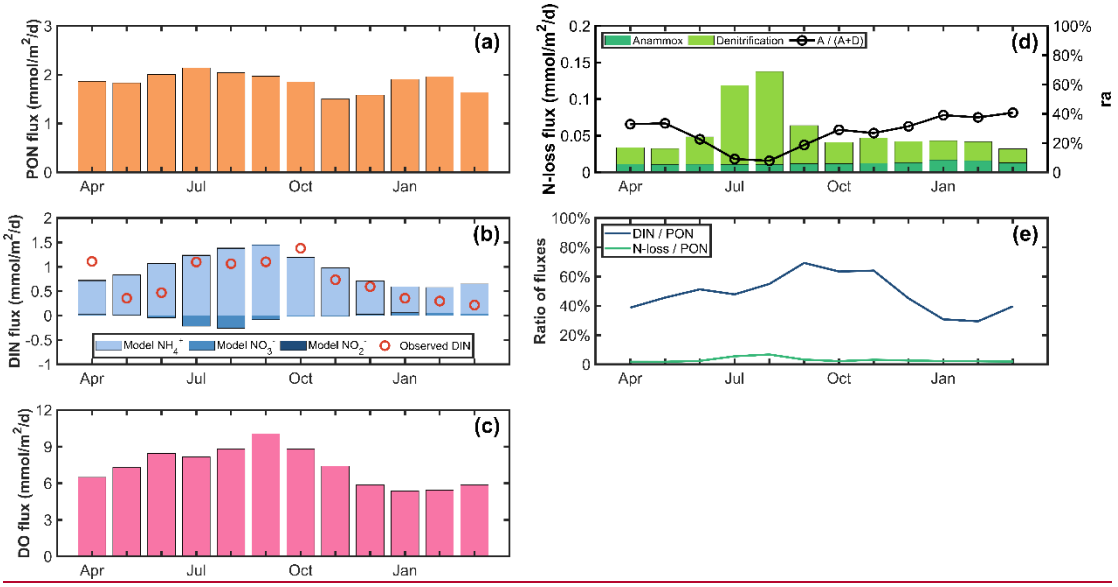

Figure 5. The fluxes of (a) PON, (b) DIN, (c) DO, (d) N-loss (N_2 and N_2O) at the sediment-water interface in the model, and (~~d~~e) the ratios of DIN and N-loss fluxes to PON flux. The red circles in (b) are the values given by observations. DIN in (b) are sum of $\mathbf{NH_4^+}$, $\mathbf{NO_2^-}$ and $\mathbf{NO_3^-}$, whose fluxes are presented in different colour in the same panel.

~~The fluxes of NH_4^+ and NO_3^- was summed up to account the flux of DIN between bottom water and sediment.~~ DIN in the Harima Nada was released from the sediment into the bottom water throughout the year, exhibiting the highest flux of 1.0437 mmol m^{-2} d^{-1} in September and the lowest flux of 0.3758 mmol m^{-2} d^{-1} in February (Figure 5b). The DIN flux and its seasonal variation given by the model exhibit a

general agreement with observations (Nakakuni et al., 2024). NH_4^+ ~~2024), although the model does not capture the observed high flux in April. The NH_4^+ and NO_3^- fluxes demonstrated comparable seasonal trends, reaching their respective maxima in September (0.61 and 0.43 mmol m^{-2} d^{-1}) and minima in February (0.20 and 0.16 mmol m^{-2} d^{-1}~~flux dominated the seasonal variability of DIN flux, reaching a maximum of 1.44 mmol m^{-2} d^{-1} in September and a minimum of 0.52 mmol m^{-2} d^{-1} in February. In contrast, NO_3^- fluxes were substantially smaller. From June to November, NO_3^- was transported from the bottom water into the sediment, with a maximum influx of 0.26 mmol m^{-2} d^{-1} in August. From December to April, NO_3^- was released from the sediment into the overlying water, with a peak of 0.06 mmol m^{-2} d^{-1} in January. NO_2^- fluxes were negligible. A slight influx into the sediment occurred in January (0.002 mmol m^{-2} d^{-1}), whereas in all other months NO_2^- was released from the sediment, with a maximum of 0.02 mmol m^{-2} d^{-1} in August. DO flux continuously supplies DO from the bottom water to the sediment and is the only source of DO for the sediment. It reached the highest value in September at 10.06 mmol m^{-2} d^{-1} and its lowest in January at 5.37 mmol m^{-2} d^{-1} (Figure 5c).

N-loss is produced through denitrification and anammox inside the sediment, which releases N_2 and N_2O to the atmosphere. N-loss flux across the sediment-water interface reached its peak of 0.~~48~~14 mmol m^{-2} d^{-1} in August and the lowest value of 0.~~39~~03 mmol m^{-2} d^{-1} in ~~February~~March (Figure ~~5c). The anammox was the main process for producing~~5d). Denitrification-derived N_2 and ~~contributed a value of around~~N_2O constituted the dominant components of N-loss flux and controlled its seasonal variability, with values ranging from 0.~~37~~02 to 0.13 mmol m^{-2} d^{-1} ~~to N_2 flux, with minimal~~. In contrast, N_2 production via anammox showed weak seasonal variation~~. Conversely, denitrification contributed to a seasonal variation of N loss flux, reaching a maximum of~~ , remaining approximately constant at 0.01~~0.09~~ mmol m^{-2} d^{-1}. Consequently, the relative contribution of anammox to N-loss flux (ra %) was lowest in August (8%) and ~~a minimum of 0.03 mmol m^{-2} d^{-1}~~highest in March~~.~~ (41%). Although N_2 was the main product of denitrification, the flux of N_2O, a potent greenhouse gas, was not negligible. It varied from 0.~~3~~19 to ~~0.9~~1.27 μmol m^{-2} d^{-1}, with a mean value of 0.~~55~~44 μmol m^{-2} d^{-1}.

The ratio of DIN flux to PON flux ($R_{DIN/PON}$) reflects the fraction of nitrogen that sinks into the sediment and later releases back to the seawater (Figure ~~5d~~5e). $R_{DIN/PON}$ increased from ~~25~~39% in ~~January~~April to a peak of ~~58~~69% in ~~June~~September, with the annual average of ~~40~~48%. The ratio of N-loss flux to PON flux ($R_{N\text{-}loss/PON}$) represented the proportion of nitrogen removed from the sediment. The highest value of

$R_{N\text{-}loss/PON}$ was ~~40~~7% in ~~June~~August while the lowest value was ~~16~~2% in ~~October~~May. The sum of $R_{DIN/PON}$ and $R_{N\text{-}loss/PON}$ ranged from ~~48~~32% in ~~October~~February to ~~98~~73% in ~~June~~September, with an annual average of ~~69~~51%. It suggested that around ~~30~~50% of the PON flux sinking from seawater was retained in the sediment on average, with this retention rate potentially reaching nearly ~~50~~70% during certain months.

3.3 The budgets of PON, NH_4^+ and NO_3^- in the sediment

The annual budgets for the ~~three~~four forms of nitrogen in the sediment of Harima Nada are estimated from the model results (Figure 6). The sinking of PON from bottom water was the source of PON in the sediment, quantified at ~~8.30~~9.50 g N m^{-2} yr^{-1}. Since the primary production in the Harima Nada in 2020 was estimated to be 41 g N m^{-2} yr^{-1} (Tada, 2021), it could be interpreted that about ~~20~~23% of the particles produced by primary production sank into the sediment. Within the deeper layers of the sediment, the burial rate of PON was ~~2.60~~3.69 g N m^{-2} yr^{-1}, representing ~~31~~39% of the PON flux into the sediment and ~~69~~% of the primary production. The rest 5.~~69~~74 g N m^{-2} yr^{-1} of PON flux into the sediment was mineralized to NH_4^+, which became the main source of NH_4^+ in the sediment.

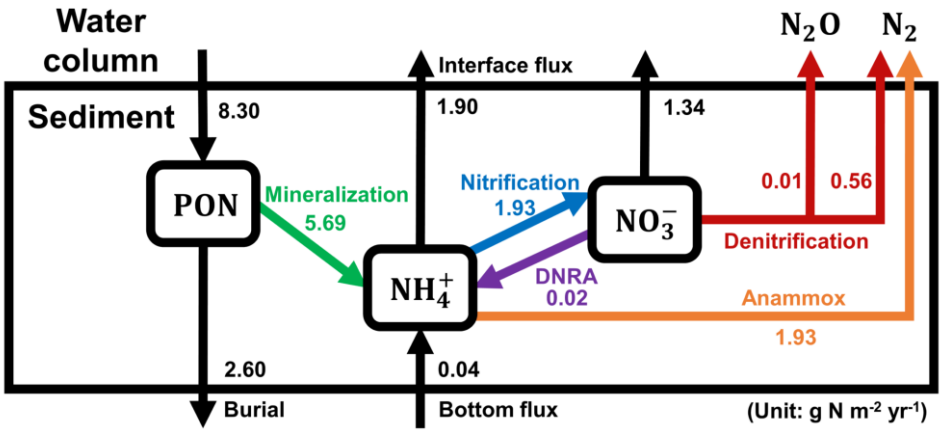

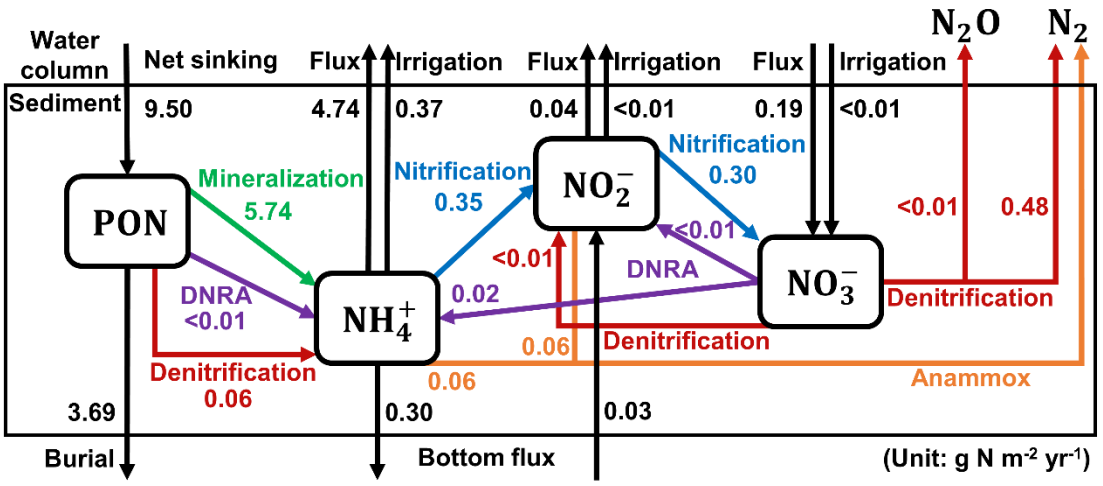

Figure 6. Nitrogen budgets in the sediment model of Harima Nada.

In addition to mineralization, ~~DNRA~~NH_4^+ was also produced ~~NH_4^+~~ via denitrification and DNRA in ~~our~~the model, ~~but its~~with the value of 0.06 g N m^{-2} yr^{-1} and 0.02 g N m^{-2} yr^{-1} ~~was two orders of magnitude lower than the amount of mineralization (5.69 g N m^{-2} yr^{-1}).~~, respectively. And 0.~~04~~30 g N m^{-2} yr^{-1} of NH_4^+ was ~~supplied from~~transferred to the deeper sediment located beneath the model domain. Furthermore, NH_4^+ has ~~three~~four sinks: the nitrification of NH_4^+ to ~~NO_3^-~~NO_2^- had a rate of ~~1.93~~0.35 g N m^{-2} yr^{-1}, the anammox of NH_4^+ to N_2 had a rate of ~~1.93~~0.06 g N m^{-2} yr^{-1}, ~~and~~ the upward NH_4^+ flux through the sediment-water interface was quantified at ~~1.90~~ 4.74 g N m^{-2} yr^{-1} and 0.37 g N m^{-2} yr^{-1} of NH_4^+ was released from the sediment by bioirrigation.

At the sediment–water interface, NO_2^- was released into the overlying water with a flux of 0.04 g N m^{-2} yr^{-1}, while bioirrigation contributed less than 0.01 g N m^{-2} yr^{-1}. Nitrification converted 0.30 g N m^{-2} yr^{-1} of NO_2^- into NO_3^-. NO_3^- inputs from the bottom water to the sediment occurred via diffusive exchange and bioirrigation, amounting to 0.19 and less than 0.01 g N m^{-2} yr^{-1}, respectively. DNRA consumed 0.02 g N m^{-2} yr^{-1} of NO_3^-, whereas denitrification produced 0.48 g N m^{-2} yr^{-1} of N_2 and N_2O. In total, nitrogen removal processes (denitrification and anammox) generated 0.54 g N m^{-2} yr^{-1} of N_2 and N_2O, corresponding to approximately 6% of the PON sinking flux. Overall, bioirrigations are much weaker than fluxes in the exchange of solutes between sediments and water, and their seasonal variations shown in Figure S5 and Text S3.

~~For the NO_3^- produced by the nitrification, it mainly had an upward flux of 1.34 g N m^{-2} yr^{-1} at the sediment-water interface and the denitrification of 0.57 g N m^{-2} yr^{-1}. The combined effects of denitrification of NO_3^- and anammox of NH_4^+ produced a N loss flux to the atmosphere amounting to~~

~~2.50 g N m^{-2} yr^{-1} (2.49 for N_2 and 0.01 for N_2O). Since this value represented over 30% of PON sinking flux to the sediment, it became an important process for removing nitrogen in the semi-enclosed inland sea.~~

4 Discussion

4.1 Factors affecting the seasonal variations of nitrogen inventories in the sediment ~~water fluxes of nitrogen~~

The model results show that the ~~fluxes~~concentrations of PON, ~~DIN~~NH_4^+, NO_2^-, NO_3^- and ~~N loss between seawater and~~DO in the sediment exhibit apparent seasonal variations. To clarify the factors controlling these seasonal variations, we carried out ~~five~~seven sensitivity experiments, in which we removed the seasonal variation of one of the following ~~five~~seven variables by substituting its monthly means with its annual mean: PON concentration (PON^{bw}), NH_4^+ concentration (NH_4^{+bw}), NO_3^- concentration (NO_3^{-bw}), ~~bottom~~ NO_2^- concentration (NO_2^{-bw}), DO concentration (DO^{bw}), and water temperature~~, and~~ in the overlying water, as well as bottom stress. Figure 7 shows the calculation results of the ~~five~~seven sensitivity experiments alongside the results described in Section 3 (referred to "Control" in Figure 7).

The concentration of PON^{bw}, bottom stress and the bottom water temperature significantly influence the seasonal variation of PON inventory in the sediment (Figure 7a). Sinking of PON^{bw} serves as the source of PON in the sediment, ~~while~~controlled by the concentration of PON^{bw} and bottom stress. The variations in bottom water temperature can change the mineralization rate in the sediment (Figure S~~3~~6a and Text ~~S3~~S4). Although these seasonal variations can directly impact the PON inventory, the extent of seasonal variation in PON inventory is relatively minor, with its value being more than two orders of magnitude smaller than the overall PON inventory.

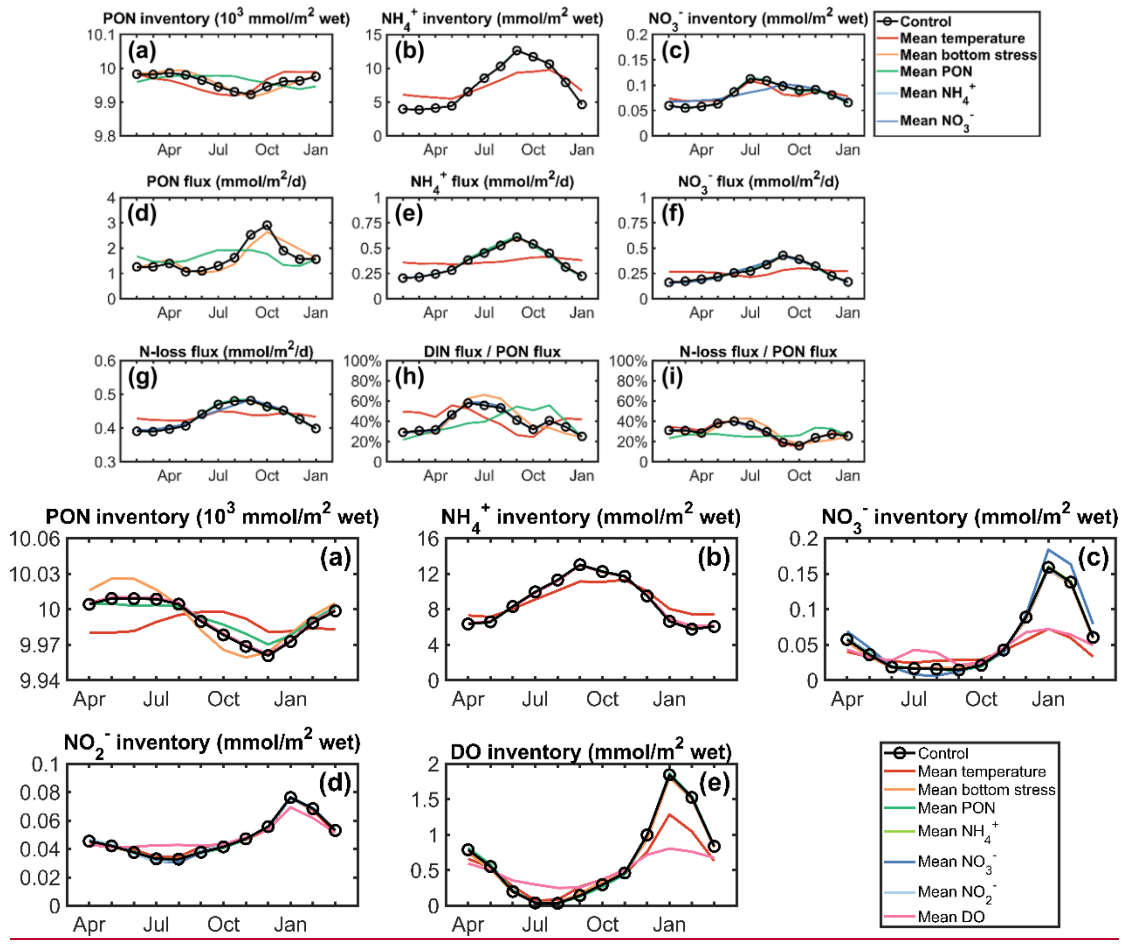

Figure 7. Comparisons of the model results among ~~six~~eight calculations (~~five~~seven sensitivity experiments and one control run). The sensitivity experiments include the cases removing the seasonal variations of PON concentration (dark green line, "Mean PON"), $\mathbf{NH_4^+}$ concentration (light ~~blue~~green line, "Mean $\mathbf{NH_4^+}$"), $\mathbf{NO_3^-}$ concentration (dark blue line, "Mean $\mathbf{NO_3^-}$"), ~~,~~ $\mathbf{NO_2^-}$ concentration (light blue line, "Mean $\mathbf{NO_2^-}$"), DO concentration (pink line, "Mean DO") and water temperature (red line, "Mean temperature") in the overlying water, as well as of the bottom stress (orange line, "Mean bottom stress"). (a) PON inventory; (b) $\mathbf{NH_4^+}$ inventory; (c) $\mathbf{NO_3^-}$ inventory; (d) ~~PON flux; (e) $\mathbf{NH_4^+}$ flux; (f) $\mathbf{NO_3^-}$ flux; (g) N-loss flux; (h) ratio of DIN flux to PON flux; (i) ratio of N-loss flux to PON flux~~$\mathbf{NO_2^-}$ inventory; (e) DO inventory.

Among the ~~5~~7 factors, only the bottom water temperature is responsible for the seasonal variations of NH_4^+ inventory (Figure 7b) as it affects the mineralization rate that produces NH_4^+ in the sediment (Figure ~~S3~~S6 and Text ~~S3). The seasonal variation of NO_3^- inventory~~S4). NH_4^+ is ~~mainly controlled by NO_3^{-bw} instead of bottom water temperature (Figure 7c). When the concentration of NO_3^{-bw} is fixed at its annual mean, a decrease in concentration enhances an increase in NO_3^- flux from the sediment~~produced primarily through mineralization and is predominantly released to the overlying water. Due to the very low NH_4^{+bw} concentration（Figure 3b）and the relatively minor contributions of other biogeochemical processes compared to mineralization (Figure ~~7f), leading to a corresponding decline in~~

~~NO_3^- inventory (Figure S4 and Text S4).~~6), bottom water temperature serves as the primary environmental factor regulating NH_4^+ inventory.

NO_3^- inventory is mainly controlled by bottom water temperature, DO^{bw}, and NO_3^{-bw} concentration (Figure 7c). High temperatures in summer enhance denitrification (Figure S6d), leading to substantial NO_3^- consumption. At the same time, low DO^{bw} concentrations limit DO supply to the sediment, thereby suppressing nitrification and further reducing NO_3^- availability (Figure S6b, c). Consequently, NO_3^- concentrations are relatively low in summer. In contrast, during winter, NO_3^- is better preserved in the sediment, resulting in higher concentrations. However, the lower NO_3^{-bw} concentration during winter also constrains its supply to the sediment. As an intermediate product of nitrification, NO_2^- is primarily controlled by DO^{bw} concentration (Figure 7d).

Since sedimentary DO is supplied exclusively from the overlying water, DO concentrations within the sediment are largely governed by DO^{bw} (Figure 7e). In winter, lower temperatures reduce the consumption of DO through mineralization, allowing more DO to be preserved within the sediment. This also explains the deeper OPD occurred in winter.

4.2 Factors affecting the seasonal variations in the sediment-water fluxes of nitrogen

The seasonal variation in concentration of PON^{bw} ~~is~~and the bottom stress are the main factors deciding the seasonal variation of PON flux across the interface between the bottom water and sediment (Figure ~~7d~~8a). High concentration of PON^{bw} ~~leads to an increased~~ increases the sinking flux of PON from seawater to sediment. ~~With the annual average value of PON^{bw} concentration as the input condition, the peak PON flux from the seawater to sediment in October disappears (Figure 3a). In such a case, an~~An inverse seasonal relationship can be discerned between PON flux ~~(the green line in Figure 7d)~~ and bottom stress (Figure ~~3e~~3h). The rise in bottom stress during the spring and winter induces the resuspension of PON at the sediment-water interface, thereby diminishing the downward PON flux.

The bottom water temperature controls not only the seasonal variations of NH_4^+ inventory in the sediment (Figure 7b) but also that of NH_4^+ flux from the sediment to the bottom water (Figure ~~7e~~8b). This is because NH_4^+ concentration in the sediment is much higher than the concentration of NH_4^{+bw}, and its variation directly determines the change of NH_4^+ flux (Figure 3b and Figure 4b). ~~Since NH_4^+ is the sole source of NO_3^- in the sediment by nitrification (Figure 6 and Figure S3b), NO_3^- flux is~~

~~consequently controlled by the bottom water temperature (Figure 7f). As a combination of NH_4^+ flux and NO_3^- flux, the seasonal variation of DIN flux is also controlled by the bottom water temperature, which is consistent with the conclusion suggested from field studies (Nakakuni et al., 2024).~~

Bottom water temperature, DO^{bw}, and NO_3^{-bw} concentration jointly drive the summer peak of NO_3^- flux into the sediment (Figure 8c). On the one hand, high temperatures in summer enhance mineralization, increasing NH_4^+ production and thereby supplying substrate for nitrification. On the other hand, high temperatures accelerate molecular diffusion, strengthening solute exchange across the sediment–water interface. However, the low DO concentration in the sediment during summer suppress nitrification, while relatively low sedimentary NO_3^- concentrations favor the flux of NO_3^- from the bottom water into the sediment. In addition, the relatively high NO_3^{-bw} concentration during summer further contributes to the enhanced downward NO_3^- flux. NO_2^- flux is comparatively small and exhibit high sensitivity to variations in bottom water temperature, as well as NO_3^{-bw}, NO_2^{-bw}, and DO^{bw} concentrations (Figure 8d).

The DO flux is primarily controlled by bottom water temperature (Figure 8e). Temperature regulates molecular diffusion and thus governs the exchange of DO across the sediment–water interface. Furthermore, the low DO^{bw} concentrations associated with the formation of the summer bottom cold water in Harima Nada also play a key role in limiting DO flux.

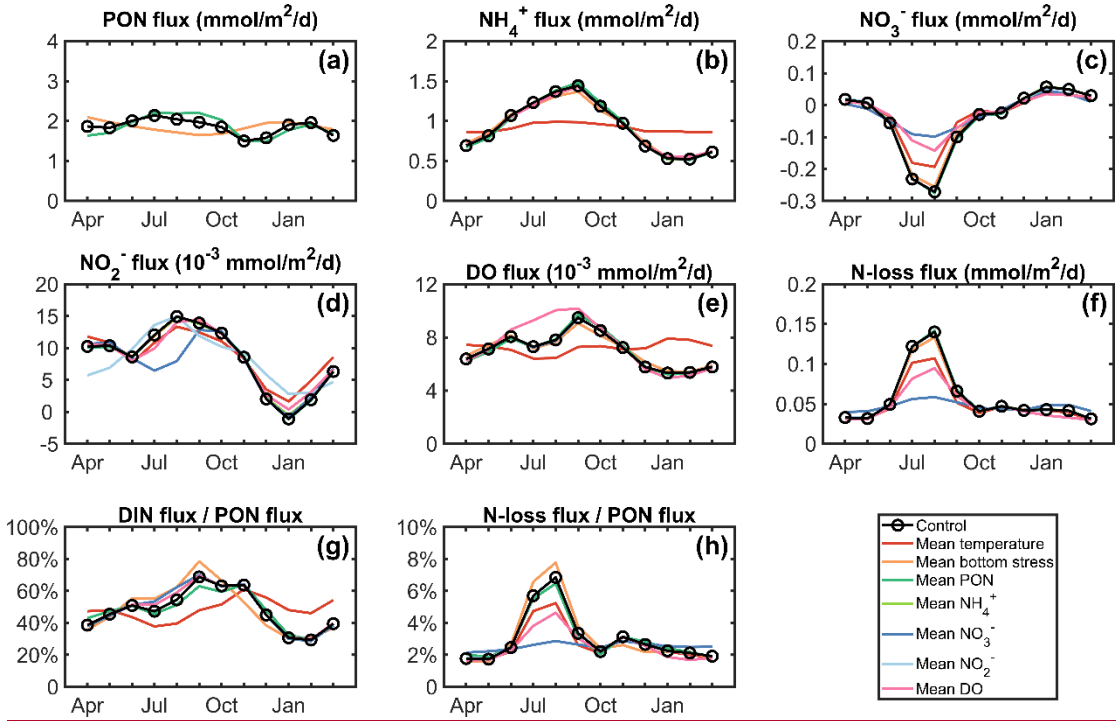

Figure 8. Comparisons of the model results among eight calculations (seven sensitivity experiments and one control run). The sensitivity experiments include the cases removing the seasonal variations of PON concentration (dark green line, "Mean PON"), NH_4^+ concentration (light green line, "Mean NH_4^+"), NO_3^- concentration (dark blue line, "Mean NO_3^-"), NO_2^- concentration (light blue line, "Mean NO_2^-"), DO concentration (pink line, "Mean DO") and water temperature (red line, "Mean temperature") in the overlying water, as well as of the bottom stress (orange line, "Mean bottom stress"). (a) PON flux; (b) NH_4^+ flux; (c) NO_3^- flux; (d) NO_2^- flux; (e) DO flux; (f) N-loss flux; (g) ratio of DIN flux to PON flux; (h) ratio of N-loss to PON flux.

The differences in the factors controlling the seasonal variation of PON and DIN fluxes indicate that a large PON flux into the sediment does not necessarily lead to a corresponding increase in DIN flux from the sediment to the bottom water. This suggests that estimating the DIN flux by using reflective boundary conditions based only on the concentration of PON^{bw}, or relying on empirical formulations that neglect bottom water temperature, may lead to considerable ~~inaccuracies~~errors in the representing of the seasonal variation in DIN flux.

~~N-loss occurs through denitrification and anammox, and is consequently closely associated with the inventories of NH_4^+ and NO_3^- in the sediment. Our calculation shows that the seasonal variation in N-loss flux mainly depends on the bottom water temperature and NO_3^{-bw} (Figure 7g). Since anammox is the dominant process for producing N_2 in the sediment, the bottom temperature, rather than NO_3^{-bw}, has a greater impact on the seasonal variation of N-loss flux.~~

The N-loss flux is dominated by denitrification (Figure 6). However, the NO_3^- concentration in summer sediments is low and needs to be supplemented by NO_3^{-bw}. This results in NO_3^- flux contributing to the summer peak of denitrification. Therefore, its seasonal variability of N-loss flux is controlled by factors similar to those governing NO_3^- flux (Figure 8f). $R_{DIN/PON}$ and $R_{N\text{-}loss/PON}$ are two important parameters for comprehending the nitrogen cycle in the semi-enclosed inland sea. The seasonal variation of $R_{DIN/PON}$ is likely controlled by ~~PON^{bw} and~~ bottom water temperature and bottom stress (Figure ~~7h). The annual mean~~8g), while that of ~~bottom temperature appears to advance the peak of $R_{DIN/PON}$, whereas the annual mean of PON^{bw} delays this peak. Conversely,~~ $R_{N\text{-}loss/PON}$ is ~~only~~ affected by ~~PON^{bw}~~bottom water temperature, DO^{bw}, and NO_3^{-bw} concentration (Figure ~~7i). The absence of an effect from bottom temperature effect on $R_{N\text{-}loss/PON}$ is caused by the relatively smaller range of N-loss flux compared to PON flux.~~ 8h).

4.2 Influences of the DO profiles on nitrogen cycle in the sediment

The availability of DO has an important impact on the nitrogen cycle in the pore water. The DO concentration has a maximum value at the top of the pore water and diminishes with increasing depths (Devol, 2015). Consequently, the vertical profile of DO concentration in the sediment is characterized by a surface maximum concentration (DO_{max}) and the oxygen penetration depth (OPD). To assess the sensitivity of our model results to the specified DO concentration in the sediment, we conducted two groups of numerical experiments to clarify the effects of DO_{max} (GROUP I) and OPD (GROUP II) on the nitrogen cycle in the sediment.

According to the observed data obtained from the Ministry of the Environment of Japan (https://water-pub.env.go.jp/water-pub/mizu-site/mizu/kouiki/dataMap.asp), the average concentration of DO in the bottom water in the Seto Inland Sea ranged from 429 to 714 mmol m^{-3} in the past 40 years, which is far beyond the DO concentration in the fluff layer as the input data (84 mmol m^{-3}). Therefore, in GROUP I of the numerical experiments, DO_{max} was varied within the range of 60–140 mmol m^{-3}, while OPD was maintained at a constant value of 2 mm. The model results showed that there were no significant changes in the nitrogen inventories of the three types of nitrogen or their fluxes at the sediment-water interface (figures not given). The reason is that DO is not a limiting factor for nitrogen cycle within the aerobic zone of the upper 3 mm of sediment when DO_{max} is maintained between 60–140 mmol m^{-3}.

It has been reported that the OPD in inland sediment can reach around 5 mm (Dale et al., 2011). In the five simulations of GROUP II, OPD was changed from 1 to 5 mm in 1 mm increments, while DO_{max} was maintained at a constant level of 80 mmol m^{-3}. The vertical profiles of DO concentration were derived through exponential fitting. The model results indicated that OPD has clear influences on NO_3^- inventory, NH_4^+ flux, NO_3^- flux and N loss flux (Figures 8c, e, f, g). An increase of OPD facilitates the occurrence of nitrification in an expanded aerobic zone, leading to a greater conversion of NH_4^+ to NO_3^-. Since NH_4^+ mainly remains in the deeper sediment layers (Figure 4b), nitrification occurring in the surface sediment has a minimal impact on NH_4^+ inventory (Figure 8b). However, it can significantly reduce NH_4^+ flux at the sediment-water interface (Figure 8e). NO_3^- inventory in the sediment increases by 218% as OPD rises from 1 to 5 mm (Figure 8c). The increase in NO_3^- inventory subsequently enhances both NO_3^- flux and denitrification, resulting in a higher N loss flux (Figures 8f and g). However, there is minimal difference in the NH_4^+, NO_3^-, and N loss fluxes among the cases with OPD

values of 3, 4, and 5 mm, indicating that beyond a certain critical threshold, the influence of OPD on these fluxes becomes negligible. Therefore, if the OPD exhibits seasonal variation between 1 and 3 mm, it will have a significant impact on the seasonal variation of nitrogen fluxes; if the OPD remains consistently deeper than 3 mm, its impact is less pronounced. Moreover, since an increase in OPD has opposing effects on NH_4^+ and NO_3^- fluxes, its overall influence on DIN flux is minimal.

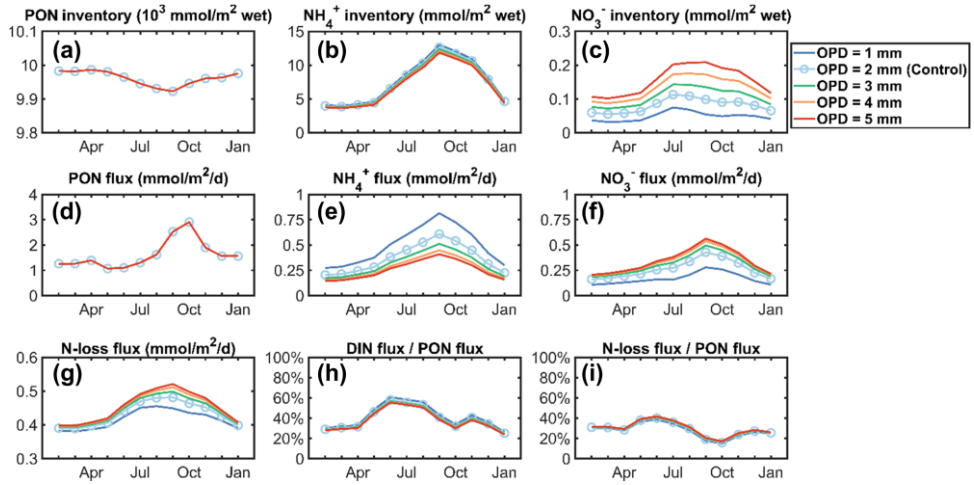

Figure 8. The effect of OPD depth on the nitrogen cycle in sediment: (a) PON inventory; (b) NH_4^+ inventory; (c) NO_3^- inventory; (d) PON flux; (e) NH_4^+ flux; (f) NO_3^- flux; (g) N-loss flux; (h) ratio of DIN flux to PON flux; (i) ratio of N-loss to PON flux.

4.3 Comparisons with other coastal seas

Numerous studies have evaluated the nitrogen fluxes at the sediment-water interface, yielding varying conclusions (Zhou et al., 2017; Sun et al., 2021; Canion et al., 2014; Lin et al., 2017; De Vittor et al., 2012; Mu et al., 2017; Rich et al., 2020; Dale et al., 2022; Bohlen et al., 2011; Ratmaya et al., 2022; Zhou et al., 2022). In this subsection, we compare the fluxes of NH_4^+, NO_3^- and N-loss calculated by our sediment model with the values reported in these studies for different coastal seas (Table 3).

Table 3. Benthic fluxes (mmol m^{-2} d^{-1}) reported in some regions; positive values represent the release from sediment to water.

Flux	Value		Location	References
NH_4^+	1.53	to 1.62	Northern Adriatic Sea	(De Vittor et al., 2012)
	0.16	to 1.39	Mauritanian upwelling region	(Dale et al., 2022)
	0.12	to 5.3	Vilaine Bay	(Ratmaya et al., 2022)
	-0.1077	to 0.219	Areas off eastern Taiwan	(Zhou et al., 2017)
	-0.71	to 0.14	Bohai Bay	(Mu et al., 2017)
	-0.1	to 0.066	Yellow Sea and East China Sea	(Zhou et al., 2022)
	0	to 4	Peruvian upwelling region	(Bohlen et al., 2011)
	0.0867	to 0.4722	Taranto Gulf	(De Vittor et al., 2015)
	0.~~22~~52	to ~~0.63~~1.44	Harima Nada	This study
NO_3^-	-0.46	to -0.26	Northern Adriatic Sea	(De Vittor et al., 2012)
	-3	to -0.1	Mauritanian upwelling region	(Dale et al., 2022)
	-0.62	to 0.46	Vilaine Bay	(Ratmaya et al., 2022)
	-0.241	to 0.00005	Areas off eastern Taiwan	(Zhou et al., 2017)
	1.43	to 2.26	Bohai Bay	(Mu et al., 2017)
	-3.43	to 0.082	Yellow Sea and East China Sea	(Zhou et al., 2022)
	-3.8	to -0.3	Peruvian upwelling region	(Bohlen et al., 2011)
	4.8	to 8.8	Taranto Gulf	(De Vittor et al., 2015)
	-0.~~17~~26	to 0.~~43~~06	Harima Nada	This study
N_2	2.7	to 544.3	Chinese marginal seas	(Sun et al., 2021)

28.70	to 420.49	East China Sea	(Lin et al., 2017)
0.2	to 2.8	Arctic shelf	(Canion et al., 2014)
1322.4	to 2683.2	Peru margin	(Rich et al., 2020)
0.~~40~~03	to 0.~~48~~14	Harima Nada	This study

615

616 NH_4^+ is released from the sediment to the bottom water in our study area. ~~It is~~ Such upward flux has been
617 commonly observed ~~and has been reported~~ in other coastal regions, including Northern Adriatic Sea (De
618 Vittor et al., 2012), Vilaine Bay (Ratmaya et al., 2022) and Eastern Taiwan (Zhou et al., 2017). ~~The~~
619 ~~difference between our study area and these coastal waters is that the sediment in our region also serves~~
620 ~~as a source of NO_3^- for the overlying seawater. The NO_3^- concentrations observed in the bottom water~~
621 ~~of Harima Nada were not always higher than that in the pore water.~~
622 NO_3^- flux exhibits pronounced seasonal variability in both magnitude and direction. In Harima Nada, the
623 formation of strong stratification in summer promotes the appearance of hypoxic conditions and limits
624 the supply of DO to the sediment. As a result, nitrification is suppressed and cannot effectively replenish
625 sedimentary NO_3^-. Meanwhile, the seasonal peak in bottom water NO_3^- concentration promotes the
626 transport of NO_3^- from the water column into the sediment. Although the seasonal reversal in flux
627 direction differs from that reported for Vilaine Bay, the underlying controlling mechanisms are similar
628 (Ratmaya et al., 2022). Therefore, the seasonal variations in temperature and bottom water NO_3^-
629 concentration jointly regulate the magnitude and direction of nitrate flux. ~~Consequently, NO_3^- produced~~
630 ~~by nitrification in the sediment can be released into the water column.~~ In contrast, in areas such as the
631 offshore of eastern Taiwan, the sediment continuously absorbs NO_3^- from the overlying water because
632 of the lower concentration of NO_3^- in the pore water compared to the overlying water (Zhou et al., 2017).
633 The N-loss flux is an important sink of nitrogen in the sediment of the Harima Nada, constituting about
634 ~~30~~6% of the sinking flux of PON into the sediment. The flux of N_2 estimated in our study is about one
635 to two orders of magnitude smaller than the values reported in other areas such as the East China Sea
636 and Arctic shelf. This discrepancy may be attributed to higher bacterial activity in those areas or to
637 elevated concentrations of organic matter and NO_3^- in the sediment (Sun et al., 2021; Canion et al., 2014;
638 Lin et al., 2017; Rich et al., 2020). Our results indicate that denitrification is the dominant pathway
639 contributing to nitrogen removal, consistent with numerous previous studies (Teng and Lin, 2024;
640 Dalsgaard et al., 2005). In the sediment, NO_2^-, as an intermediate, remains at relatively low
641 concentrations and is insufficient to sustain high rates of anammox. Consequently, the availability of
642 NO_2^- primarily governs the seasonal variability of the relative contribution of anammox to N-loss flux.
643 In particular, summer hypoxia leads to low NO_2^- production, which suppresses anammox while favoring
644 denitrification, resulting in the lowest relative contribution of anammox during this period.

~~Our results indicate that the anammox rate is approximately three times greater than the denitrification rate. However, some previous studies reported that anammox contributes a smaller N_2 flux compared to denitrification (Teng and Lin, 2024; Dalsgaard et al., 2005). The first reason for this difference is the lower maximum NO_3^- concentration or shallower NO_3^- penetration in Harima-Nada sediments, which leads to a denitrification rate lower than that in those regions. In addition, the low concentration of NH_4^+ in the sediment of those regions, even as the same scale as the NO_3^- concentration, limits the rate of anammox and reduces the contribution to N_2. In contrast, NH_4^+ concentration in the sediment in this study was significantly higher than NO_3^- concentration, thereby enhancing the potential rate of anammox (Canion et al., 2014; Rich et al., 2020). Another reason is that the sediment thickness utilized in our model was set at 10 cm, whereas most conventional observations sampled only the surface sediment, potentially underestimating the contribution of anammox in deeper layers. Usually, NH_4^+ concentrations in pore water are much lower in the surface layer compared to deeper layers, resulting in a reduced anammox reaction rate in the 0–5 cm layer relative to the 5–10 cm layer. When concentrating on the upper 5 cm of sediment, our model results suggest that the anammox rate constitutes a smaller proportion of N_2, accounting for less than 50% in summer (Figure S5 and Text S5), which is consistent with some observations (Teng and Lin, 2024; Dalsgaard et al., 2005).~~

5 Conclusions

This study developed a one-dimensional vertical sediment model to investigate the seasonal variations in the direction and magnitude of nitrogen fluxes at the sediment-water interface in semi-enclosed inland seas, and to reveal the controlling mechanisms of various environmental factors on these variations. Utilizing continuous observational data from a typical semi-enclosed inland sea for validation, we found that the flux of PON settling from the bottom water to the sediment is the main source of nitrogen in the sediment, with its seasonal variation governed by the PON concentration in the bottom water~~.~~ and bottom stress. Due to the regeneration of a substantial amount of NH_4^+ in the sediment, NH_4^+ is continuously released from the sediment to the overlying water, with its seasonal variation ~~being~~controlled by bottom water temperature~~ controlled~~. Temperature influences the mineralization rate, which subsequently affects NH_4^+ flux through NH_4^+ inventory in the sediment. ~~NO_3^- flux at the interface is directed upward~~

~~in an oligotrophic water column, and its seasonal variation is also temperature-controlled. The influence of temperature over NH_4^+ inventory in the sediment is transmitted to NO_3^- inventory through nitrification, thereby affecting NO_3^- flux.~~Under the combined control of bottom water temperature and NO_3^- concentration, both the direction and magnitude of NO_3^- flux exhibited significant seasonal variations. This results in the seasonal variation of DIN flux returning from the sediment to the water being unrelated to the PON flux, as ~~these two~~they are controlled by different environmental factors with distinct seasonal patterns. This finding suggests that neglecting to consider bottom water temperature and ~~PON concentration~~nitrogen concentrations in reflective boundary conditions or empirical formulas may lead to varying degrees of misestimation when calculating the seasonal variation of DIN flux at the sediment-water interface.

~~The rate of nitrogen removal in sediments with low nitrate levels, possibly found in oligotrophic environments, is primarily controlled by anammox. Moreover, traditional observations are limited by the sampling depth of sediments, which may result in an underestimation of the contribution of anammox in deeper sediment layers. Our findings indicate that the maximum concentration of DO in sediments, which ranged from 60 to 140~~ Denitrification is the main process of the nitrogen removal and contributes to the seasonal variation of N-loss. However, the overall nitrogen removal amount is relatively low, possibly due to the low NO_3^- concentration in the bottom water caused by the oligotrophic environment of Harima Nada.~~mmol m^{-3}, has a negligible impact on sediment nitrogen cycling. However, seasonal variations in oxygen penetration depth, which ranges from 1 to 3 mm, can significantly influence nitrogen fluxes at the sediment-water interface.~~ In addition, this model is mainly suited for semi-enclosed inland seas dominated by muddy sediments and does not account for the advection of pore water flow in sandy sediments. In practice, this process can be incorporated by adjusting the vertical velocity in the solute transport equation. Overall, this model can be widely applied to investigate nitrogen cycling-related issues in nearshore muddy sediments. Moreover, by investigating the seasonal variations of nitrogen cycling in semi-enclosed inland sea sediments and their controlling factors, it can provide a basis for governance and management support for environmental issues such as coastal eutrophication.

In future research, we will expand upon this study by integrating it with long-term observational data to investigate the effects of prolonged changes in aquatic environments, such as eutrophication and seawater warming, on sediment nitrogen cycling and nitrogen flux at the sediment-water interface.

Code, data, or code and data availability

The source code of the numerical model used in this study is available on request. Please contact the corresponding author.

Author contributions

Zhaosen Wu: conceptualization, methodology, software, validation, visualization, writing (original draft preparation). Xinyu Guo: formal analysis, methodology, resources, supervision, writing (review and editing). Jie Shi: supervision, writing (review and editing). Xiaokun Ding: methodology, software. Masatoshi Nakakuni: data curation, investigation, resources. Kuninao Tada: data curation, investigation, resources.

Competing interests

The authors declare that they have no conflict of interest.

Supporting Information

Supporting Information is available free of charge at the Biogeosciences website.

Acknowledgement

This research was performed by the Environment Research and Technology Development Fund (JPMEERF20255002) of the Environmental Restoration and Conservation Agency Provided by the Ministry of Environment of Japan. We thank Dr. Akihiko Morimoto and Dr. Naoki Yoshie who worked

724 in the Center for Marine Environmental Studies, Ehime University, Japan and provided valuable
725 suggestions for our research. Z. Wu thanks the China Scholarship Council (CSC) and the Ministry of
726 Education, Culture, Sports, Science and Technology, Japan (MEXT) for a project on Joint
727 Usage/Research Center, Leading Academia in Marine and Environmental Research (LaMer) for
728 supporting his study in Japan.
729
730

References

Akbarzadeh, Z., Laverman, A. M., Rezanezhad, F., Raimonet, M., Viollier, E., Shafei, B., and Van Cappellen, P.: Benthic nitrite exchanges in the Seine River (France): An early diagenetic modeling analysis, Sci Total Environ, 628-629, 580-593, 10.1016/j.scitotenv.2018.01.319, 2018.

Berelson, W. M., McManus, J., Severmann, S., and Reimers, C. E.: Benthic flux of oxygen and nutrients across Oregon/California shelf sediments, Cont. Shelf Res., 55, 66-75, 10.1016/j.csr.2013.01.009, 2013.

Berner, R.: Early diagenesis: a theoretical approach: Princeton, 1980.

Bohlen, L., Dale, A. W., Sommer, S., Mosch, T., Hensen, C., Noffke, A., Scholz, F., and Wallmann, K.: Benthic nitrogen cycling traversing the Peruvian oxygen minimum zone, Geochim. Cosmochim. Acta, 75, 6094-6111, 10.1016/j.gca.2011.08.010, 2011.

Boudreau, B. P., Mucci, A., Sundby, B., Luther, G. W., and Silverberg, N.: Comparative diagenesis at three sites on the Canadian continental margin, J. Mar. Res., 56, 1259-1284, 10.1357/002224098765093634, 1998.

Boynton, W. R., Ceballos, M. A. C., Bailey, E. M., Hodgkins, C. L. S., Humphrey, J. L., and Testa, J. M.: Oxygen and Nutrient Exchanges at the Sediment-Water Interface: a Global Synthesis and Critique of Estuarine and Coastal Data, Estuaries Coasts, 41, 301-333, 10.1007/s12237-017-0275-5, 2017.

Canion, A., Overholt, W. A., Kostka, J. E., Huettel, M., Lavik, G., and Kuypers, M. M.: Temperature response of denitrification and anaerobic ammonium oxidation rates and microbial community structure in Arctic fjord sediments, Environ Microbiol, 16, 3331-3344, 10.1111/1462-2920.12593, 2014.

Capet, A., Meysman, F. J. R., Akoumianaki, I., Soetaert, K., and Grégoire, M.: Integrating sediment biogeochemistry into 3D oceanic models: A study of benthic-pelagic coupling in the Black Sea, Ocean Modelling, 101, 83-100, 10.1016/j.ocemod.2016.03.006, 2016.

Chang, P.-H., Guo, X., and Takeoka, H.: A numerical study of the seasonal circulation in the Seto Inland Sea, Japan, Journal of Oceanography, 65, 721-736, 10.1007/s10872-009-0062-4, 2009.

Chen, S., Gao, D., Zhang, J., Zheng, Y., Li, X., Dong, H., Yin, G., Han, P., Liang, X., Liu, M., Müller, C., and Hou, L.: Gross nitrogen transformations in intertidal sediments of the Yangtze Estuary: Distribution patterns and environmental controls, Geoderma, 429, 10.1016/j.geoderma.2022.116233, 2023.

759 Dale, A. W., Clemens, D., Dähnke, K., Korth, F., Wankel, S. D., Schroller-Lomnitz, U., Wallmann, K.,
760 and Sommer, S.: Nitrogen cycling in sediments on the NW African margin inferred from N and O
761 isotopes in benthic chambers, Frontiers in Marine Science, 9, 10.3389/fmars.2022.902062, 2022.
762 Dale, A. W., Sommer, S., Bohlen, L., Treude, T., Bertics, V. J., Bange, H. W., Pfannkuche, O., Schorp,
763 T., Mattsdotter, M., and Wallmann, K.: Rates and regulation of nitrogen cycling in seasonally hypoxic
764 sediments during winter (Boknis Eck, SW Baltic Sea): Sensitivity to environmental variables, Estuar.
765 Coast. Shelf Sci., 95, 14-28, 10.1016/j.ecss.2011.05.016, 2011.
766 Dalsgaard, T., Thamdrup, B., and Canfield, D. E.: Anaerobic ammonium oxidation (anammox) in the
767 marine environment, Research in microbiology, 156, 457-464, 2005.
768 De Vittor, C., Relitti, F., Kralj, M., Covelli, S., and Emili, A.: Oxygen, carbon, and nutrient exchanges
769 at the sediment–water interface in the Mar Piccolo of Taranto (Ionian Sea, southern Italy), Environmental
770 Science and Pollution Research, 23, 12566-12581, 10.1007/s11356-015-4999-0, 2015.
771 De Vittor, C., Faganeli, J., Emili, A., Covelli, S., Predonzani, S., and Acquavita, A.: Benthic fluxes of
772 oxygen, carbon and nutrients in the Marano and Grado Lagoon (northern Adriatic Sea, Italy), Estuarine,
773 Coastal and Shelf Science, 113, 57-70, 10.1016/j.ecss.2012.03.031, 2012.
774 Devol, A. H.: Denitrification, Anammox, and N2 Production in Marine Sediments, Annu. Rev. Mar. Sci.,
775 7, 403-423, 10.1146/annurev-marine-010213-135040, 2015.
776 Ding, X., Guo, X., Zhang, C., Yao, X., Liu, S., Shi, J., Luo, C., Yu, X., Yu, Y., and Gao, H.: Water
777 conservancy project on the Yellow River modifies the seasonal variation of Chlorophyll-a in the Bohai
778 Sea, Chemosphere, 254, 126846, 10.1016/j.chemosphere.2020.126846, 2020.
779 Han, A., Kao, S. J., Lin, W., Lin, Q., Han, L., Zou, W., Tan, E., Lai, Y., Ding, G., and Lin, H.: Nutrient
780 Budget and Biogeochemical Dynamics in Sansha Bay, China: A Coastal Bay Affected by Intensive
781 Mariculture, Journal of Geophysical Research: Biogeosciences, 126, 10.1029/2020jg006220, 2021.
782 Huang, F., Lin, X., Hu, W., Zeng, F., He, L., and Yin, K.: Nitrogen cycling processes in sediments of the
783 Pearl River Estuary: Spatial variations, controlling factors, and environmental implications, CATENA,
784 206, 105545, https://doi.org/10.1016/j.catena.2021.105545, 2021.
785 Huettel, M., Berg, P., and Kostka, J. E.: Benthic Exchange and Biogeochemical Cycling in Permeable
786 Sediments, Annu. Rev. Mar. Sci., 6, 23-51, 10.1146/annurev-marine-051413-012706, 2014.

Ichimi, K., Tada, K., and Montani, S.: The phytoplankton assemblage of the past and present in the Seto Inland Sea-the expectation from sediment core samples, Aquabiology, 27, 214～221, 2005.

Ishii, D., Yanagi, T., and Sasakura, S.: Long-term trends in the occurrence of red tides in the Seto Inland Sea, Japan, Oceanography in Japan, 23, 217-236, 10.5928/kaiyou.23.6_217, 2014.

Jäntti, H. and Hietanen, S.: The Effects of Hypoxia on Sediment Nitrogen Cycling in the Baltic Sea, Ambio, 41, 161-169, 10.1007/s13280-011-0233-6, 2012.

Kalvelage, T., Lavik, G., Lam, P., Contreras, S., Arteaga, L., Löscher, C. R., Oschlies, A., Paulmier, A., Stramma, L., and Kuypers, M. M. M.: Nitrogen cycling driven by organic matter export in the South Pacific oxygen minimum zone, Nature Geoscience, 6, 228-234, 10.1038/ngeo1739, 2013.

Khalil, M. A. K. and Rasmussen, R. A.: The global sources of nitrous oxide, Journal of Geophysical Research: Atmospheres, 97, 14651-14660, 10.1029/92jd01222, 2012.

Kuhrts, C., Seifert, T., and Fennel, W.: Modeling Transport of Fluff Layer Material in the Baltic Sea, Hydrobiologia, 554, 25-30, 10.1007/s10750-005-1003-x, 2006.

Laima, M., Maksymowska-Brossard, D., Sauriau, P.-G., Richard, P., Girard, M., Gouleau, D., and Joassard, L.: Fluff deposition on intertidal sediments: effects on benthic biota, ammonium fluxes and nitrification rates, Biogeochemistry, 61, 115-133, 10.1023/a:1020264414924, 2002.

Laurent, A., Fennel, K., Wilson, R., Lehrter, J., and Devereux, R.: Parameterization of biogeochemical sediment–water fluxes using in situ measurements and a diagenetic model, Biogeosciences, 13, 77-94, 10.5194/bg-13-77-2016, 2016.

Lee, J.-Y., Tett, P., Jones, K., Jones, S., Luyten, P., Smith, C., and Wild-Allen, K.: The PROWQM physical–biological model with benthic–pelagic coupling applied to the northern North Sea, J. Sea Res., 48, 287-331, https://doi.org/10.1016/S1385-1101(02)00182-X, 2002.

Leng, Q., Guo, X., Zhu, J., and Morimoto, A.: Contribution of the open ocean to the nutrient and phytoplankton inventory in a semi-enclosed coastal sea, Biogeosciences, 20, 4323-4338, 10.5194/bg-20-4323-2023, 2023.

Leynaert, A., Longphuirt, S. N., An, S., Lim, J.-H., Claquin, P., Grall, J., Kwon, B. O., and Koh, C. H.: Tidal variability in benthic silicic acid fluxes and microphytobenthos uptake in intertidal sediment, Estuarine, Coastal and Shelf Science, 95, 59-66, 10.1016/j.ecss.2011.08.005, 2011.

Lin, X., Liu, M., Hou, L., Gao, D., Li, X., Lu, K., and Gao, J.: Nitrogen Losses in Sediments of the East China Sea: Spatiotemporal Variations, Controlling Factors, and Environmental Implications, Journal of Geophysical Research: Biogeosciences, 122, 2699-2715, 10.1002/2017jg004036, 2017.

Liu, H. and Yin, B.: Annual cycle of carbon, nitrogen and phosphorus in the Bohai Sea: A model study, Cont. Shelf Res., 27, 1399-1407, 10.1016/j.csr.2007.01.015, 2007.

Liu, S. M., Li, L. W., Zhang, G. L., Liu, Z., Yu, Z., and Ren, J. L.: Impacts of human activities on nutrient transports in the Huanghe (Yellow River) estuary, Journal of Hydrology, 430-431, 103-110, 10.1016/j.jhydrol.2012.02.005, 2012.

Liu, X., Stock, C. A., Dunne, J. P., Lee, M., Shevliakova, E., Malyshev, S., and Milly, P. C. D.: Simulated Global Coastal Ecosystem Responses to a Half-Century Increase in River Nitrogen Loads, Geophysical Research Letters, 48, e2021GL094367, https://doi.org/10.1029/2021GL094367, 2021.

Lønborg, C. and Markager, S.: Nitrogen in the Baltic Sea: Long-term trends, a budget and decadal time lags in responses to declining inputs, Estuarine, Coastal and Shelf Science, 261, 107529, https://doi.org/10.1016/j.ecss.2021.107529, 2021.

McTigue, N. D., Gardner, W. S., Dunton, K. H., and Hardison, A. K.: Biotic and abiotic controls on co-occurring nitrogen cycling processes in shallow Arctic shelf sediments, Nature Communications, 7, 13145, 10.1038/ncomms13145, 2016.

Mei Liu, S., Wei Li, L., and Zhang, Z.: Inventory of nutrients in the Bohai, Cont. Shelf Res., 31, 1790-1797, 10.1016/j.csr.2011.08.004, 2011.

Mu, D., Yuan, D., Feng, H., Xing, F., Teo, F. Y., and Li, S.: Nutrient fluxes across sediment-water interface in Bohai Bay Coastal Zone, China, Mar. Pollut. Bull., 114, 705-714, 10.1016/j.marpolbul.2016.10.056, 2017.

Nakakuni, M., Yamaguchi, H., Ichimi, K., and Tada, K.: Seasonal variation in pore water nutrients and their fluxes from the bottom sediments in Harima Nada, Seto Inland Sea, Journal of Oceanography, 80, 219-232, 10.1007/s10872-024-00719-7, 2024.

Niemistö, J., Kononets, M., Ekeroth, N., Tallberg, P., Tengberg, A., and Hall, P. O. J.: Benthic fluxes of oxygen and inorganic nutrients in the archipelago of Gulf of Finland, Baltic Sea – Effects of sediment resuspension measured in situ, J. Sea Res., 135, 95-106, 10.1016/j.seares.2018.02.006, 2018.

Pastor, L., Cathalot, C., Deflandre, B., Viollier, E., Soetaert, K., Meysman, F. J. R., Ulses, C., Metzger, E., and Rabouille, C.: Modeling biogeochemical processes in sediments from the Rhône River prodelta area (NW Mediterranean Sea), Biogeosciences, 8, 1351-1366, 10.5194/bg-8-1351-2011, 2011.

Radtke, H., Lipka, M., Bunke, D., Morys, C., Woelfel, J., Cahill, B., Böttcher, M. E., Forster, S., Leipe, T., Rehder, G., and Neumann, T.: Ecological ReGional Ocean Model with vertically resolved sediments (ERGOM SED 1.0): coupling benthic and pelagic biogeochemistry of the south-western Baltic Sea, Geoscientific Model Development, 12, 275-320, 10.5194/gmd-12-275-2019, 2019.

Ratmaya, W., Laverman, A. M., Rabouille, C., Akbarzadeh, Z., Andrieux-Loyer, F., Barillé, L., Barillé, A.-L., Le Merrer, Y., and Souchu, P.: Temporal and spatial variations in benthic nitrogen cycling in a temperate macro-tidal coastal ecosystem: Observation and modeling, Cont. Shelf Res., 235, 10.1016/j.csr.2022.104649, 2022.

Rich, J. J., Arevalo, P., Chang, B. X., Devol, A. H., and Ward, B. B.: Anaerobic ammonium oxidation (anammox) and denitrification in Peru margin sediments, J. Mar. Syst., 207, 10.1016/j.jmarsys.2018.09.007, 2020.

Sayama, M., Sohma, A., and Takasugi, Y.: Experimental analysis of the effect of flow velocity on oxygen dynamics near the water-sediment interface in a coastal zone., Proceedings of Coastal Engineering, 49, 996-1000, 10.2208/proce1989.49.996, 2002.

Soetaert, K., Herman, P. M. J., and Middelburg, J. J.: A model of early diagenetic processes from the shelf to abyssal depths, Geochim. Cosmochim. Acta, 60, 1019-1040, 10.1016/0016-7037(96)00013-0, 1996.

Sun, L., Wang, C., Yu, H., Liu, D., Houlton, B. Z., Wang, S., Zeng, X., Bai, E., Fang, Y., and Jia, Y.: Biotic and Abiotic Controls on Dinitrogen Production in Coastal Sediments, Glob. Biogeochem. Cycle, 35, 10.1029/2021gb007069, 2021.

Tada, K.: Primary Production, Nutrients and Nutrient Release from Bottom Sediments in Coastal Water, Journal of Water Environment Society of Japan, 44, 137-141, 2021.

Teng, Z. and Lin, X.: Sediment nitrates reduction processes affected by non-native Sonneratia apetala plantation in South China, Sci. Total Environ., 906, 167523, 2024.

Thamdrup, B.: New Pathways and Processes in the Global Nitrogen Cycle, Annual Review of Ecology, Evolution, and Systematics, 43, 407-428, 10.1146/annurev-ecolsys-102710-145048, 2012.

Tong-u-dom, S., Morimoto, A., Leng, Q., and Guo, X.: Seasonal variation in the current field and development of bottom cold water in Harima-Nada, Journal of Oceanography, 80, 1-20, 10.1007/s10872-023-00702-8, 2023.

Tong-U-Dom, S., Morimoto, A., Guo, X., Leng, Q., Yoshie, N., Tada, K., Ichimi, K., Yamaguchi, H., and Nakakuni, M.: Lower trophic ecosystem dynamics in the eastern part of the Seto Inland Sea and their response to changes in nutrient supply from the rivers, Prog. Oceanogr., 239, 10.1016/j.pocean.2025.103565, 2025.

Umlauf, L., Klingbeil, K., Radtke, H., Schwefel, R., Bruggeman, J., and Holtermann, P.: Hydrodynamic Control of Sediment-Water Fluxes: Consistent Parameterization and Impact in Coupled Benthic-Pelagic Models, Journal of Geophysical Research: Oceans, 128, 10.1029/2023jc019651, 2023.

Wang, J., Zhao, L., Fan, R., and Wei, H.: Scaling relationships for diffusive boundary layer thickness and diffusive flux based on in situ measurements in coastal seas, Prog. Oceanogr., 144, 1-14, 10.1016/j.pocean.2016.03.001, 2016.

Wang, X. H.: Tide-Induced Sediment Resuspension and the Bottom Boundary Layer in an Idealized Estuary with a Muddy Bed, Journal of Physical Oceanography, 32, 3113-3131, 10.1175/1520-0485(2002)032<3113:Tisrat>2.0.Co;2, 2002.

Wilson, S. T., Al-Haj, A. N., Bourbonnais, A., Frey, C., Fulweiler, R. W., Kessler, J. D., Marchant, H. K., Milucka, J., Ray, N. E., Suntharalingam, P., Thornton, B. F., Upstill-Goddard, R. C., Weber, T. S., Arévalo-Martínez, D. L., Bange, H. W., Benway, H. M., Bianchi, D., Borges, A. V., Chang, B. X., Crill, P. M., del Valle, D. A., Farías, L., Joye, S. B., Kock, A., Labidi, J., Manning, C. C., Pohlman, J. W., Rehder, G., Sparrow, K. J., Tortell, P. D., Treude, T., Valentine, D. L., Ward, B. B., Yang, S., and Yurganov, L. N.: Ideas and perspectives: A strategic assessment of methane and nitrous oxide measurements in the marine environment, Biogeosciences, 17, 5809-5828, 10.5194/bg-17-5809-2020, 2020.

Yamamoto, T., Orimoto, K., Asaoka, S., Yamamoto, H., and Onodera, S.-i.: A Conflict between the Legacy of Eutrophication and Cultural Oligotrophication in Hiroshima Bay, Oceans, 2, 546-565, 10.3390/oceans2030031, 2021.

Yang, J.-Y. T., Hsu, T.-C., Tan, E., Lee, K., Krom, M. D., Kang, S., Dai, M., Hsiao, S. S.-Y., Yan, X., and Zou, W.: Sedimentary processes dominate nitrous oxide production and emission in the hypoxic zone off the Changjiang River estuary, Sci. Total Environ., 827, 154042, 2022.

Yi, Y., Gao, Y., Wu, X., Jia, W., and Liu, Q.: Modeling the effect of artificial flow and sediment flux on the environment and plankton of an estuary, International Journal of Sediment Research, 38, 335-348, https://doi.org/10.1016/j.ijsrc.2023.02.001, 2023.

Zhang, X., Ward, B. B., and Sigman, D. M.: Global Nitrogen Cycle: Critical Enzymes, Organisms, and Processes for Nitrogen Budgets and Dynamics, Chem Rev, 120, 5308-5351, 10.1021/acs.chemrev.9b00613, 2020.

Zhang, X., Zhang, Q., Yang, A., Hou, L., Zheng, Y., Zhai, W., and Gong, J.: Incorporation of microbial functional traits in biogeochemistry models provides better estimations of benthic denitrification and anammox rates in coastal oceans, Journal of Geophysical Research: Biogeosciences, 123, 3331-3352, 2018.

Zhou, F., Gao, X., Zhang, Y., Yuan, H., Song, J., Liu, K., Yang, B., and Zhuang, W.: Potential mobility of inorganic nutrients and its controls at the sediment-water interface in the main path of Kuroshio Current off eastern Taiwan, Mar Pollut Bull, 119, 270-276, 10.1016/j.marpolbul.2017.04.002, 2017.

Zhou, N., Zhang, G. L., and Liu, S. M.: Nutrient exchanges at the sediment-water interface and the responses to environmental changes in the Yellow Sea and East China Sea, Mar Pollut Bull, 176, 113420, 10.1016/j.marpolbul.2022.113420, 2022.

Zhu, J., Guo, X., Shi, J., and Gao, H.: Dilution characteristics of riverine input contaminants in the Seto Inland Sea, Mar. Pollut. Bull., 141, 91-103, 10.1016/j.marpolbul.2019.02.029, 2019.